An EpCAM/Trop2 mechanostat differentially regulates individual and collective behaviour of human carcinoma cells

Azam Aslemarz[1,2], Marie Fagotto-Kaufmann[1,4], Artur Ruppel[3,5], Christine Fagotto-Kaufmann[1], Martial Balland[3], Paul Lasko[2] and François Fagotto[1]

[1]CRBM, University of Montpellier and CNRS, Montpellier 34293, France

[2]Dept. of Biology, McGill University, Montreal, QC, Canada H3A1B1.

[3]LIPHY, UMR5588, University of Grenoble, 38400 Grenoble, France

[4]current address: Department of Neurobiology, University of Stuttgart, 70569 Stuttgart, Germany

[5]current address: CRBM, University of Montpellier and CNRS, Montpellier 34293

Correspondence to François Fagotto, email: francois.fagotto@crbm.cnrs.fr

Abstract

EpCAM is well-known as a carcinoma associated cell surface protein, but its potential role in cancer metastasis remains unclear. EpCAM is known, however, to downregulate myosin-dependent contractility, a key parameter involved in cell adhesion and migration. We investigate here the morphogenetic impact of EpCAM levels in epithelial breast cancer cells, using spheroids of MCF7 cells as an in vitro model. We also interrogate the role of Trop2, a close relative of EpCAM, co-expressed in most epithelial cells including MCF7 cells. EpCAM depletion stimulates spheroid spreading, while it represses single cell migration. Intriguingly, Trop2 depletion led to the exact opposite phenotype from EpCAM depletion in terms of single cell migration, spheroid cohesiveness and spreading. All our observations converge to an antagonistic effect of EpCAM and Trop2 on the process of "wetting" a substrate, here both matrix and neighboring cells. Using a combination of cell biological and biophysical approaches, we show that while EpCAM and Trop2 both contribute to moderate cell contractility, their depletions differentially impact the balance between tensions at cell-medium, cell-cell and cell-matrix interfaces, fully accounting for the wetting phenotypes. Consistently, EpCAM and Trop2 show partial differential enrichment at the corresponding interfaces. Differential distribution and antagonistic loss-of-function phenotypes are also observed in two other breast cancer cell lines with very different characteristics, suggesting that these are general properties of these two regulators. Our data are consistent with a simple model in which the EpCAM-Trop2 pair acts as a mechanostat that tunes local cortical tension, thus influencing a spectrum of behaviours, from single cell migration to tissue cohesiveness and collective migration.

Introduction

Contractility of the actomyosin cellular cortex is a central determinant of cell and tissue adhesive and migratory properties. Understanding how contractility is controlled at the global and local scales is thus key to a mechanistic explanation of morphogenetic processes, including cancer metastasis. In this context, EpCAM is a particularly intriguing candidate regulator. EpCAM, also called TACSTD1, is a cell surface protein specifically expressed in epithelial tissues, and highly overexpressed in most human carcinomas [1,2]. It is an important cancer biomarker for diagnostic and therapeutic purposes [3]. While the name EpCAM (Epithelial Cell Adhesion Molecule) was given based on its proposed function as a homotypic cell adhesion molecule [4,5], this function has been strongly questioned by more recent studies (reviewed in [6,7]. EpCAM is currently rather viewed as a regulator of intracellular signalling, impacting on proliferation [8,9] as well as on physical cell properties. The latter activity relies on its ability to downregulate myosin contractility [10–14], providing an obvious putative link between EpCAM and cancer metastasis that remains to be established.

The role of EpCAM in cancer invasion is unclear: In vitro studies have brought conflicting results, consistent with either pro-adhesive or anti-adhesive, pro-migratory or anti-migratory activities (reviewed in [6]). EpCAM is downregulated upon epithelial-mesenchymal transition (EMT) [15–17], yet may be itself required for EMT [15,18,19]. Of note, the classical view that posed EMT as a necessary and key step in cancer invasiveness is currently a matter of debate. There is emerging evidence that, at least in some cases, the most invasive cells may have only undergone limited EMT, and still display many aspects of the epithelial cells from which they derive[20–22]. Along these lines, circulating tumour cell lines with high metastatic potential happen to be EpCAM positive [23,24].

A second related gene, called Trop2 or TACSTD2 is co-expressed with EpCAM in all epithelia, except in the intestine. EpCAM and Trop2 constitute a gene family on their own, Trop2 being the result of the duplication of the EpCAM gene that occurred in reptilians, at the root of amniote evolution. Human EpCAM and Trop2 have high sequence similarity between themselves, and with EpCAM of lower vertebrates. While direct comparative studies are rare, and data on their cellular and molecular properties is scarce, EpCAM and Trop2 appear very similar in virtually all features examined so far, including structure and biochemical interactions [6,14]. Trop2 has been also linked to cancer, but, again, its actual role remains to be established [6,25,26].

EpCAM morphogenetic function is best understood in non-cancer systems, specifically in zebrafish and Xenopus embryos. In both systems, gain and loss-of-function (GOF and LOF) experiments unambiguously showed that EpCAM acts positively on cell-cell adhesion and motility [27,28]. In particular, EpCAM is required during gastrulation for dynamic tissue reorganization through cell-cell intercalation [27,28]. At later stages of development, loss of EpCAM eventually caused severe defects in tissue integrity [12,27]. We showed that all the EpCAM GOF and LOF embryonic phenotypes could be accounted for by its ability to downregulate myosin activity [12,28]. At the molecular level, EpCAM directly binds and inhibits the novel class of PKC kinases (nPKC), and through it, it represses phosphorylation of myosin light chain (pMLC) by the nPKC-PKD-Raf-Erk-MLCK pathway [12]. Importantly, the positive effect of EpCAM on cadherin-mediated adhesion turned out to be a secondary effect of its regulation of myosin contractility [12]. Myosin repression through nPKC interaction appears conserved in human EpCAM and Trop2 [12]. Consistent with EpCAM function as moderator of contractility, its loss in a rare human intestinal disorder called congenital tufting enteropathy (CTE) leads to disruption of the epithelium [29], due again to myosin overactivation and uncontrolled tension of the actomyosin cortex [10,13]. A recent study on the migration of isolated intestinal Caco2 cells proposed an additional/alternative role of EpCAM in spatial regulation of RhoA and myosin activity via fast recycling endosomes [11]. The significance of this phenomenon in the context of the intact epithelium remains to be evaluated.

Since EpCAM expression is highest in carcinomas, it is fair to predict that its role in controlling myosin activity should be relevant for cancer metastasis. However, due to the multiplicity and complexity of myosin functions, one can hardly predict *a priori* how its up- or downregulation will impact on adhesion and migration in various cell types and under different conditions [6,6]. In an attempt to clarify the role of EpCAM in a cancer context, we chose breast epithelial MCF7 cells as a well-established model of carcinoma cells expressing high EpCAM [30,31]. MCF7 cells were a particularly suitable general example to address such question: The expression of EpCAM and of Trop2 are moderately high, representative of an average range found not only in breast, but

also colon or lung cancer cell lines (Expression Atlas, https://www.ebi.ac.uk/gxa), and still in the order of magnitude of what normal epithelia express. Furthermore, MCF7 cells display robust E-cadherin-mediated cell-cell adhesion as well as good migratory activity. We evaluated the impact of EpCAM levels at the cell and tissue scale, and we systematically characterized the effect on myosin contractility and adhesion, using a combination of cellular and biophysical approaches. EpCAM and Trop2 are thought to be at least partly redundant [6,32,33], and Trop2 expression could partially rescue CTE defects [34]. Yet, the conservation of the two genes throughout amniotes argues for distinct functions, but direct experimental comparison at the cellular level has been missing so far. Thus, we thought it to be important to include Trop2 in this study and characterize both molecules side by side.

We show that, beyond its general role in myosin downregulation, EpCAM differently impacts adhesion and migration depending on the context, here in particular depending on whether cells are isolated or part of a tissue. Furthermore, while our data confirmed that EpCAM and Trop2 share most properties, starting with their common role in inhibiting myosin, we made the unexpected discovery that they actually show counter-balancing contributions to adhesion and motility. The analysis of cellular and biophysical parameters has highlighted how relatively modest differences in the balance of cellular tensions can deeply impact the morphogenetic outcome. Extension of the study to HCC1500 and MDA-MD-453, two other breast cancer lines with very different characteristics, indicate that differential localization and antagonistic effect on cell behaviour are general properties of the EpCAM/Trop2 pair.

Results

EpCAM depletion increases spreading of MCF7 spheroids and their cohesiveness, while Trop2 depletion has the opposite effect

In order to investigate the role of EpCAM in collective tissue behaviour, we used spheroids of breast cancer MCF7 cells as an in vitro model that mimics a solid tumor [35]. These spheroids were placed on a soft matrix of fibrillar collagen I as a physiologically relevant ECM [36]. The collagen gel was about 20-50µm thick and sufficiently soft for spheroids to be capable to deform it (see convex ventral face of spheroids in Fig 1H'). Under these conditions, spheroids actively spread, which we typically imaged over 24 hrs (Fig 1A, Movie 1). Spreading of a spheroid is an integrated process that involves adhesion to extracellular matrix and collective migration, together with the ability of the tissue mass to remain coherent while allowing cells to exchange neighbours (aka cell intercalation). EpCAM was depleted by transfection of siRNA one day before starting to form the spheroids, which were laid on collagen two days later. By that stage, EpCAM depletion was close to complete and remained so until the end of the assay (S1A,C Fig). Spheroids formed from cells transfected with control siRNA spread efficiently, typically increasing their area by 3 to 4 folds (Fig 1A,E, S1 Movie). Note that the center of the spheroid tended to remain rather compact, while the periphery showed irregular contours, with cells or cell groups frequently sticking out of the cell mass (Fig 1A,H,I). EpCAM knockdown (KD) resulted in a strong, highly reproducible increase in spreading (Fig 1B,E,H, S2 Movie). After 24 hrs, spheroids had the shape of a flat pancake, only about 2-3 cells thick (Fig 1H'). Interestingly, these EpCAM KD spheroids expanded as a very cohesive sheet. While numerous protrusions emanated from the edge of the cell mass (Fig 1I), this edge was overall strikingly smooth compared to control spheroids (Fig 1H). The distinctive morphologies of control and EpCAM KD, indicative of differences in tissue cohesiveness, were quantitatively expressed as "solidity", a measurement that indicates how closely the surface can be described by a circle (Fig 1F). We validated the specificity of the KD phenotype by showing that it could be fully rescued by using MCF7 cells stably expressing a DOX-inducible EpCAM variant resistant to the siRNAs (S2A Fig). We also verified that the increased migration/spreading of siEpCAM spheroids was not due to a higher proliferation rate by running the spheroid assay in the presence of Mitomycin C (MMC), an anti-mitotic agent (S1F Fig). MMC totally blocked the cell cycle, as validated by thymidine analogue EdU incorporation (S1F' Fig). We concluded that the increased spreading upon EpCAM KD was independent of cell proliferation, but rather due to changes in morphogenetic properties. In reciprocal GOF experiments, EpCAM overexpression decreased spheroid spreading, thus opposite to the depletion phenotype (S2B Fig). One could infer from these results that EpCAM expression in MCF7 cells limits tissue spreading.

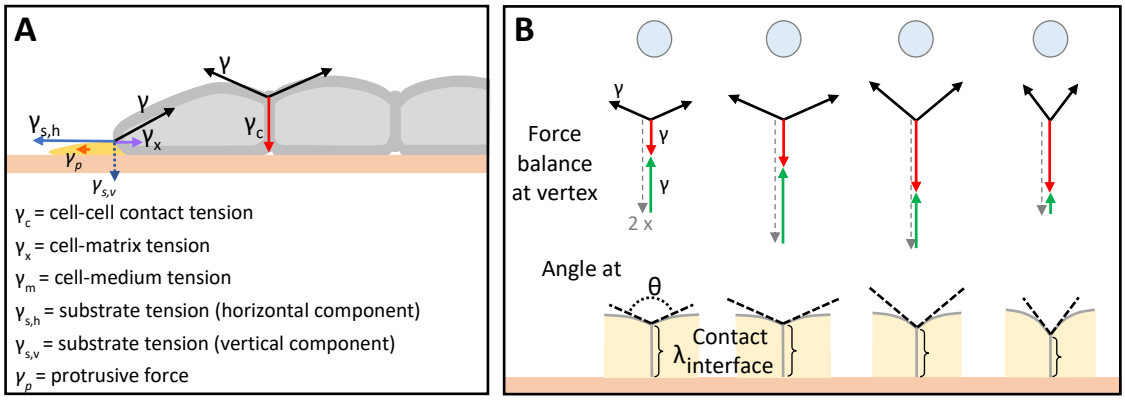

Box 1. Description of cell spreading and adhesion based on the balance of tensions at interfaces. (A) recruitment of cortical cytoskeleton and of adhesion molecules, and enhanced liThe capacity of cells to spread on a substrate, be it matrix or other cells, is strongly dependent on contractility of the actomyosin cortex, which can be viewed as analogous to the role of surface tension in the physical process of the "wetting" of a surface by a liquid [40-43]. The system can similarly be described as the balance of the tensions exerted at various interfaces, namely tension at the matrix (γ_x), at cell contact (γ_c), and along the free edges exposed to the medium (γ_m). γ_x and γ_c combine various tensions exerted at the corresponding interface. In the case of cell-cell adhesion, for instance, γ_c is the sum of the cortical tensions on each sides of the contact minus the so-called "adhesive tension" (see below). For adhesion to matrix, γ_x and γ_m are balanced by substrate tension γ_s. Note that it is customary consider the horizontal components $\gamma_{s,h}$, which is typically the one measured by techniques such as traction force microscopy. Actin polymerization within the advancing protrusion also generates a force γ_p, which may contribute to the force balance, depending on the degree of the mechanical coupling with the rest of the cytoskeleton. **(B)** Taking the case of cell-cell adhesion, expansion of an adhesive contact λ requires that contact tension γ_c is lowered compared the basal cortical tension γ_m that would otherwise act on each side of the interface (2 x γ_m). This is achieved partly by the adhesion tension resulting from the binding of adhesion molecules to their ligands (cadherin-cadherin and integrins-matrix), but mainly through an active downregulation of local actomyosin contractility along the contact interface. This latter process relies on the ability of adhesion molecules to recruit regulators of cytoskeleton remodelling. To highlight this downregulation, we introduce here a single tension vector γ_a that includes the ensemble of contributions that decrease γ_c (thus $2\gamma_m = \gamma_c - \gamma_a$). **Panel 1.** Cell geometry reflects the force balance: As shown in panel (1), a low γ_c/γ_m ratio (high γ_a) leads to a large contact interface λ, and a wide angle θ. The latter is a direct geometric readout of "adhesiveness" [46]. **Panels 2-4.** Contacts adapt to stress through a process of reinforcement, involving increased linkage of adhesion molecules to the cytoskeleton [44,59]. As shown in panel (2), cells can then maintain the same degree of adhesiveness (same angle θ) despite bearing higher tensions. Importantly, this also requires more repression of contractility along the cell-cell interface (increased γ_a), another expected effect of enhanced cadherin recruitment. Panel (3) shows the situation where higher cortical tension is not compensated by increased γ_a, resulting in a higher γ_c/γ_m ratio and lower adhesiveness (smaller angle θ). In the last example (4), γ_m remains unchanged compared to (1), but γ_a is decreased, resulting in relatively high γ_c, and thus low adhesiveness (low angle θ and shorter contact interface λ. The same principles are applicable to adhesion and spreading to the extracellular matrix, which depend on the balance between γ_x and γ_m, with spreading of cell aggregates controlled by the combination of cell-matrix and cell-cell adhesion, thus by all three tensions [39,41].

MCF7 also express Trop2. Using ectopic expression of EpCAM-GFP and Trop2-GFP to calibrate immunofluorescence (IF) signals (S3 Fig), we estimated that the surface levels of EpCAM and Trop2 were quite similar. Based on the high sequence and functional similarities between EpCAM and Trop2, and their assumed partial redundancy, one may have predicted that Trop2 could partially compensate for the loss of EpCAM, and that the double EpCAM/Trop2 KD (dKD) would potentiate the EpCAM KD phenotype. To address this question, we depleted Trop2, using two distinct Trop2 siRNA (sc-43043 and H502-003), which gave very similar results (S1B, D, E Fig)(for the rest of the study we used sc-43043). Note that Trop2 depletion was not as complete as for EpCAM (~75% versus > 95%, S1 Fig), yet phenotypes throughout this study were highly reproducible and consistent. dKD spheroids did not spread more than single EpCAM KD spheroids (Fig 1D, E-H, S1E,E' Fig, S4 Movie). Furthermore, quite unexpectedly, single Trop2 KD decreased spheroid spreading, thus opposite to the effect of EpCAM KD (Fig 1C,E-H, S3 Movie). Transient expression of Trop2-

Figure 1

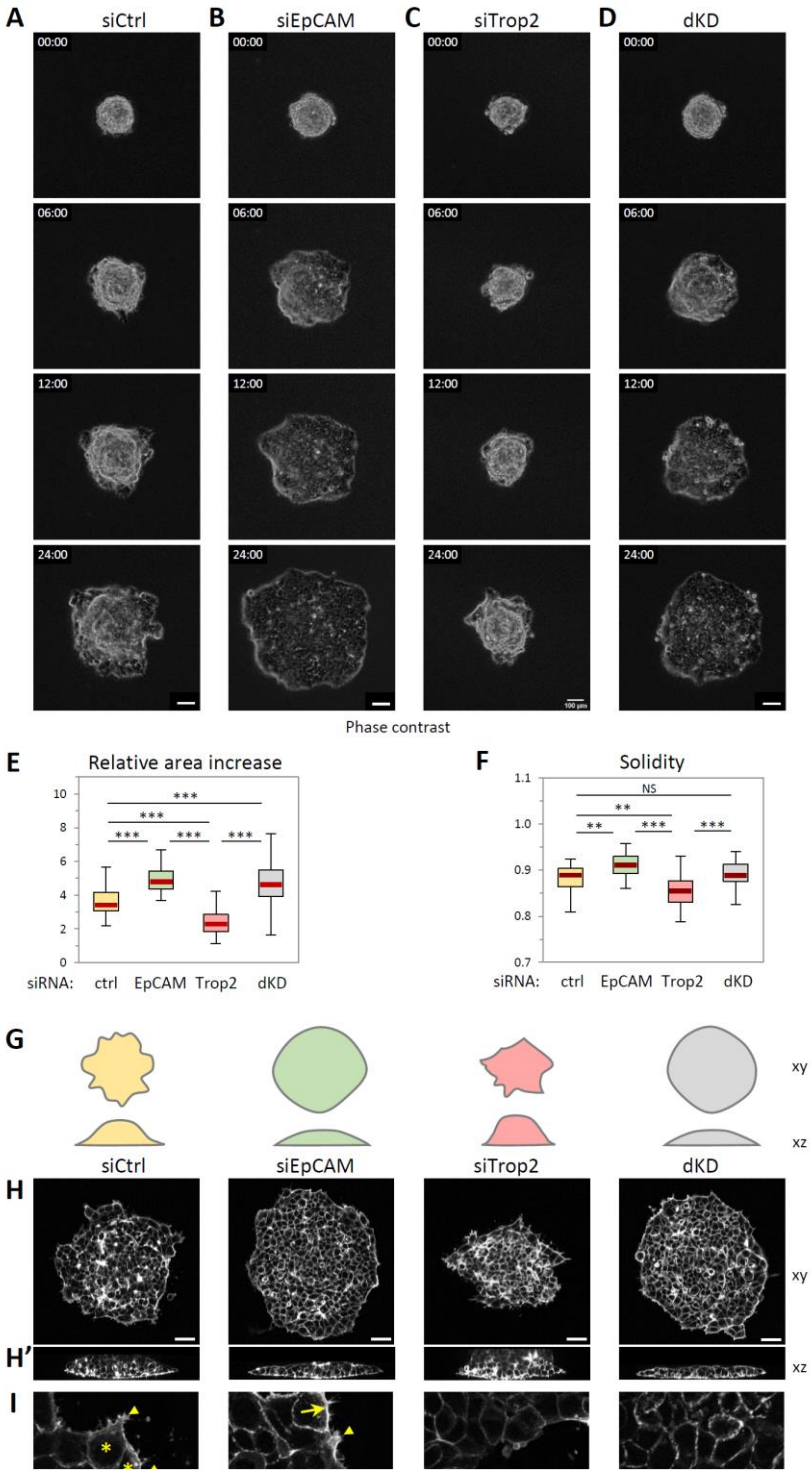

Figure 1. Cohesive collective migration of MCF7 spheroids is stimulated by EpCAM KD, but inhibited by Trop2 KD. Spheroids of transfected MCF7 cells with control, EpCAM, Trop2 and EpCAM/Trop2 siRNA were plated on a layer of fibrillar collagen gel, let adhere for 30 minutes, then phase contrast images were taken every 30min for 24hrs. **(A-D)** Images of whole spheroids at selected time points. Scale bar: 100µm. **(E)** Quantification of relative area increase after 24hrs, expressed as ratio of the final and initial areas. 45-63 spheroids from six to nine independent experiments, combining four experiments with siTrop2 sc-43043 and two with siTrop2 H502-0033, see supplemental FigS1E for separate results. Refer to S1 Data. In all figures, the box plots show the interquartile range (box limits), median (center line), and min and max values without outliers (whiskers). Statistical analysis: One-way non-parametric ANOVA (Kruskal-Wallis Test) followed by Dunn post hoc test. For all experiments presented in this study, P values are indicated as follows: * $P < 0.05$, ** $P < 0.01$, *** $P < 0.001$ and NS, not significant, only mentioned for pairs of interest. **(F)** Quantification of spheroids solidity, measured as the ratio [Area]/[Area of convex hull]. Quantification from the six experiments. Refer to S1 Data. **(G)** Schematic representation of typical spheroid morphologies in top and orthogonal views. **(H,H')** Examples of phalloidin-labelled spheroids after 24hrs spreading in top and orthogonal view. Scale bars: 100µm. **(I)** Details of spheroid edges. Maximal projection of 3 z planes, 1µm apart. Protrusions are observed in all conditions (arrowheads). However, control and Trop2 KD spheroids have numerous cells protruding out of the main cell mass (asterisks), which are rare in EpCAM KD and dKD. These are rather characterized by frequent actin cable-like structures along the spheroid edge (arrows). Scale bars: 10µm.

GFP yielded a partial but reproducible rescue (S2D Fig). The shape of Trop2 KD spheroids was very irregular, yielding a low solidity value (Fig 1F). Thus, EpCAM and Trop2 appear to play an antagonistic role in this context. While interpretation of double LOF may be ambiguous in such situation, we did include dKD in the following characterization, as this condition may help us determine properties that may be shared by EpCAM and Trop2 despite their opposite spheroid spreading phenotypes.

EpCAM and Trop2 KD have inverse effects on single MCF7 cell migration

One obvious possible cause for the spheroid migration/spreading phenotypes could be a difference in the intrinsic migratory property of the individual cells. We analyzed migration of single cells, also plated on fibrillar collagen I gel. Control MCF7 were moderately motile, with an average motility of 0.5µm/min (Fig 2A,E, S5 Movie). EpCAM KD cells spread significantly more than controls, adopting a characteristic radial shape (Fig 2B,G,H, S6 Movie). Their migration was drastically decreased compared to control (Fig 2B,E), thus opposite to the effect on spheroid spreading. On the contrary, Trop2-depleted cells tended to be rounder (Fig 2C,F,G, S7 Movie) but migrated as efficiently as control cells (Fig 2C,E Fig). dKD cells were closer to EpCAM KD cells, both in terms of spread morphology and low migration (Fig 2D-H Fig, S8 Movie). In conclusion, EpCAM KD and Trop2 KD caused the exact opposite effect on single cell migration than on spheroid spreading. However, the morphology of the single cells, flatter for EpCAM KD, rounder for Trop2 KD, strikingly paralleled the degree of spreading of the corresponding spheroids. Note that numerous highly dynamic protrusions were observed under all conditions, both in single cells (S5 Fig and S5-6 Movies), and at the periphery of spheroids (Fig 1H", S3 Fig, S5 Fig, S1-S4 Movies). Although we do not exclude subtle differences in the dynamics of these protrusions, this would be unlikely to account for the EpCAM KD and Trop2 KD phenotypes, since the single cell migration phenotypes were opposite to the spheroid spreading phenotypes. More likely targets were myosin-dependent processes, i.e. contractility of the cell cortex, cell-cell adhesion and matrix adhesion, which would in turn impact on the ability to spread and to migrate, individually or collectively.

EpCAM and Trop2 depletions both lead to upregulation of myosin activity

We asked if EpCAM KD impacted on myosin activity by probing for phosphorylated myosin light chain (pMLC). Because we wanted to detect potentially subtle local changes in myosin activation at the cell cortex, and perform the analysis in the actual context of spheroids spreading on soft collagen, we favoured quantitative IF over Western blot. Whole mount IF of spheroids showed that EpCAM KD indeed significantly increased total cortical pMLC (Fig 3A,C). pMLC was also increased in Trop2 KD, reaching levels comparable to EpCAM KD (Fig 3A and C). pMLC was also high in dKD, but not significantly different from single depletions (Fig 3A,C). We could conclude that both EpCAM and Trop2 KD indeed led to higher myosin activity. Note that differences in pMLC distribution between the free edge and cell contacts were observed, which will be presented below, and represented a strong hint for preferential sites of overactivation in response to one or the other depletions.

We functionally tested whether nPKC and myosin II, respectively the immediate and the downstream targets of EpCAM repression, were involved in the EpCAM KD spheroid spreading phenotype, using two well-established chemical inhibitors, calphostin and blebbistatin (S4A,B Fig). In the presence of either of these inhibitors, spreading of siEpCAM spheroids was reduced in a dose-dependent manner, close to the levels of controls (S4B Fig). Calphostin and blebbistatin also further inhibited spreading of wild type spheroids (S4B Fig). While these experiments did not establish whether EpCAM acted upstream or in parallel to nPKC, the results were coherent with the known nPKC/myosin-inhibiting function of EpCAM. The same inhibitors, tested over a range of concentrations, failed to rescue spreading of Trop2 KD (not shown). This negative result was not surprising considering the complex roles of actomyosin contractility, and may simply indicate that global nPKC/myosin inhibition was more successful at compensating for EpCAM depletion than for Trop2 depletion in these particular experimental settings. A likely hypothesis that we explored in the rest of

the study was that EpCAM and Trop2 differentially influenced the balance between the various myosin-dependent tensions that control cell and tissue properties

Figure 2

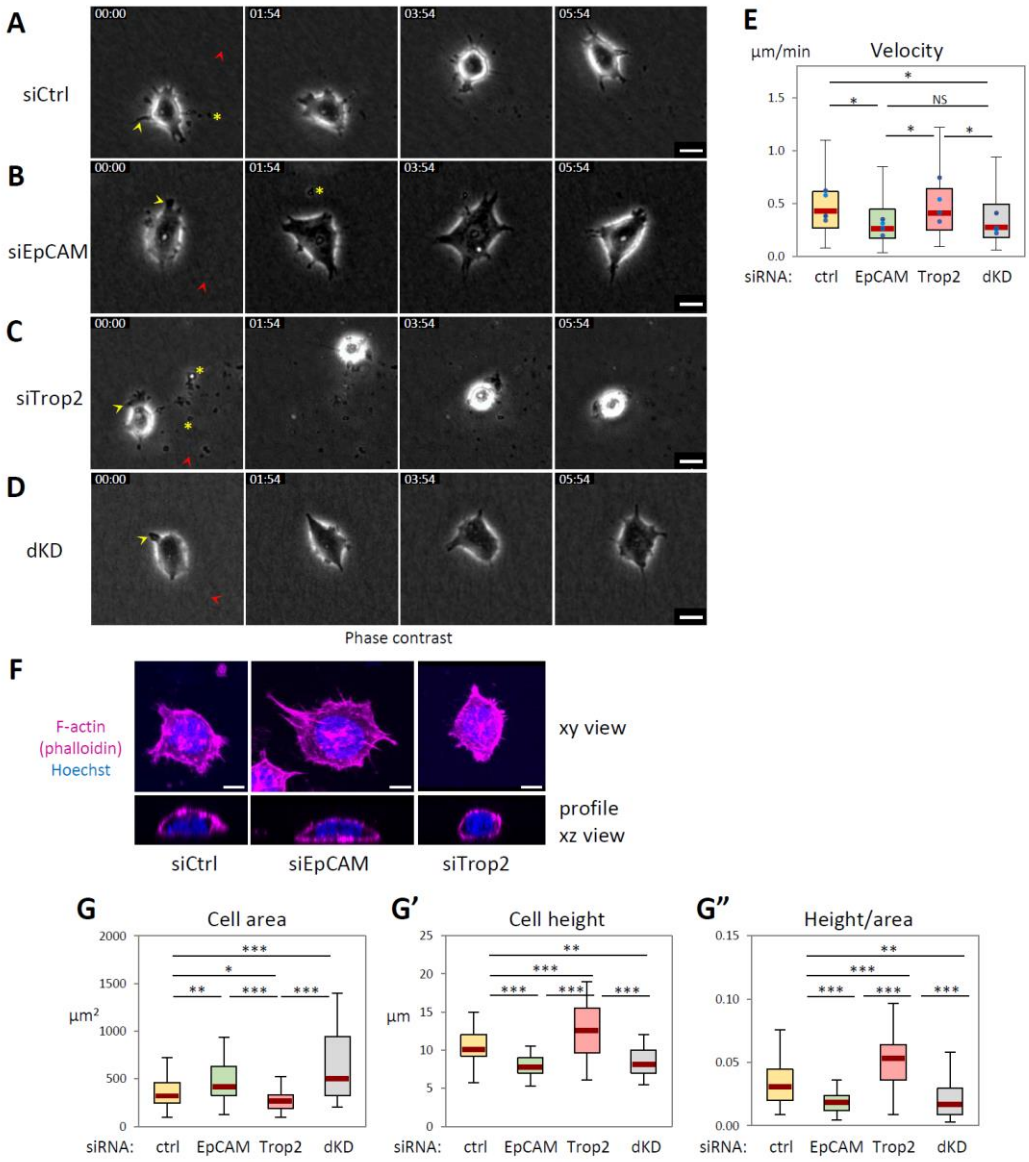

Figure 2. A-E. Single cell migration is impaired by EpCAM KD, but not Trop2 KD. Phase contrast time lapse movies MCF7 cells plated on collagen gel, and were recorded for 15 hrs. **(A-D)** Representative cells at four time points (see Movies 1-4). All cells emit multiple active protrusions (yellow arrowheads). Compared to control cells, EpCAM KD cells spread more, but migrate significantly less. Trop2 KD cells tend to be much rounder, with a much smaller contact area with the matrix, but actively migrate. dKD cells are more similar to EpCAM KD, also flatter and less migratory. Asterisks: The small dark vesicles on the substrate are protrusion remnants left behind by the migrating cells. They are trivially more abundant in fields of actively migrating cells. Red arrowheads: Collagen fibers are visible, and their distortion by cells pulling on the matrix is obvious on the corresponding movies. Scale bar: 15µm. **(E)** Quantification of average velocity. Three independent experiments (150-200 cells). Refer to S1 Data. One-way non-parametric ANOVA (Kruskal-Wallis Test) on experiment averages followed by Dunn post-hoc test. **(F-G) Effect of EpCAM and Trop2 KD on single cell morphology**. **F.** Typical examples of control, EpCAM and Trop2-depleted cells. Dissociated cells laid on collagen gel were stained with phalloidin and Hoechst and imaged by confocal microscopy. Top panels show maximal horizontal projection, the lower panel a slice from the orthogonal projection. Scale bars: 10µm. **G.** Quantification of cell area, cell height, and calculation of height/area ratio. For each condition, 95, 82, 62 and 26 cells from three independent experiments. Refer to S1 Data. One-way ANOVA followed by Tukey-HSD post-hoc test.

EpCAM and Trop2 KD have common and distinct effects on local myosin recruitment and adhesive contacts

A good approach to grasp the role of cortical actomyosin contractility is to use the well-established biophysical analogy with the wetting properties of a liquid on a surface [37–43]. Box 1 presents a simplified summary of this biophysical view of cell spreading and adhesion, and introduces the concept of "adhesiveness" used in this study. The increased, respectively decreased spreading upon EpCAM KD and Trop2 KD was suggestive that these molecules indeed acted on the "wetting" properties of the tissue (Fig 1G,H'). Furthermore, the exact same changes in morphology were observed at the single cell level (Fig 2F-G) (as well as for small groups of cells, see below Fig 4A'''), indicating that a similar balance of tensions operated at the different scales of organization. We set up to extensively characterize the effect of EpCAM and Trop2 depletions on the actomyosin cortex and adhesive structures. We present first general data from spheroids, then a more detailed analysis at the cellular level using small groups of cells (spanning a range of 2-10 cells), as well as single cells, all laid on soft collagen. We then went on to measure the actual tensions by a series of biophysical measurements.

As mentioned above, pMLC distribution in spheroids showed striking patterns: EpCAM KD and Trop2 KD both caused a general rise in pMLC signal, but the signal in siEpCAM spheroids was particularly strong along the free edge (Fig 3A,D and S5A Fig), suggestive of formation of actomyosin "cables" that could contribute to the smoothness of the circumference (Fig 1B and F). The signal at edges was less prominent in siTrop2 spheroids (Fig 3A,D, S5A Fig). Importantly, both depletions led to markedly higher E-cadherin signal (Fig 3B,E). However, when comparing pMLC and E-cadherin, the relative ratio was significantly higher in Trop2 KD compared to EpCAM KD (Fig 3F). As mentioned in Box 1, cadherin recruitment upon increased tension is a hallmark of reinforcement of cadherin-dependent cell-cell adhesion [44,45], and cadherin levels correlate with adhesiveness [43,46]. dKD spheroids also showed enriched pMLC at the edges and high E-cadherin, not significantly different from single depletions (Fig 3A-F).

As preliminary note on the analysis of groups of MCF7 cells on soft collagen, we should stress that they did form fully polarized structures with well delimited apical adherens junctions (the same was true for spheroids). E-cadherin, although often more concentrated near the dorsal side, was broadly distributed along the contact interface (Fig 4A,A'''). Consistent with the capacity of cadherins to downregulate tension [43], most of the contacts showed little to no detectable pMLC signal (Fig 4A', concave yellow arrowheads). These features, together with the extreme variability of cell morphologies and contact geometries made it vain to compare raw parameters such as total cadherin or pMLC levels. Instead, since myosin and cadherins tend to concentrate at sites where most tension is exerted, we opted for a determination of the peak intensity for E-cadherin at the cell-cell contact and, for pMLC, at contacts as well as at the free edges exposed to the medium. This approach turned out to be robust over the vast range of cell topologies, and yielded several important results.

Firstly, similar to spheroids, EpCAM KD and Trop2 KD led to increased pMLC at both contacts and free edges (Fig 4A-C), further supporting a global increase of cortical contractility. Second, there was again a clear difference in relative enrichment: pMLC was increased in the same proportion at cell contacts and free edges of EpCAM KD groups, as evident from the unchanged contact/edge ratio (Fig 4D), while the increase was significantly stronger at contacts for Trop2 KD (Fig 4C,D). Phalloidin signal was also increased proportionally at contact and edges of siEpCAM groups, and highest at contacts in Trop2 KD (Fig 4A'',G,H). Altogether, data on both spheroids and groups of cells were indicative of a fundamental difference in the balance of tensions, tilted more toward cell contacts for Trop2 KD. Again, both EpCAM KD and Trop2 KD led to markedly higher E-cadherin signal (Fig 3A and E), indicating that MCF7 cells were capable to adjust cell-cell adhesion to increased tension upon loss of EpCAM or Trop2. However, when comparing pMLC and E-cadherin, the relative ratio was higher in Trop2 KD compared to EpCAM KD (Fig 4F). As for dKD, pMLC tended to be highest at edges, indicating that both proteins contributed to downregulate tension at this interface. Otherwise values for dKD were most similar to EpCAM KD, except for low F-actin. Note that we should take with caution the results for this latter condition, the highly heterogenous morphology of these dKD cells making quantification less accurate.

In summary, data from both spheroids and small cell groups coincided: They supported the common role of EpCAM and Trop2 in moderating cortical myosin, both at the free edge and at cell-cell contacts, consistent with the known function of Xenopus EpCAM [12]. Importantly, however, they revealed two potentially key differences, a proportionally higher increase of pMLC at contacts compared to edges in Trop2 KD, and a lower E-cadherin recruitment. Based on the principles enunciated above (Box 1), these observations indicated that Trop2 KD resulted in proportionally more contact tension, consequently less adhesiveness, compared to EpCAM KD. As we will see below, measurements of tension and adhesiveness cells confirmed this effect.

Figure 3

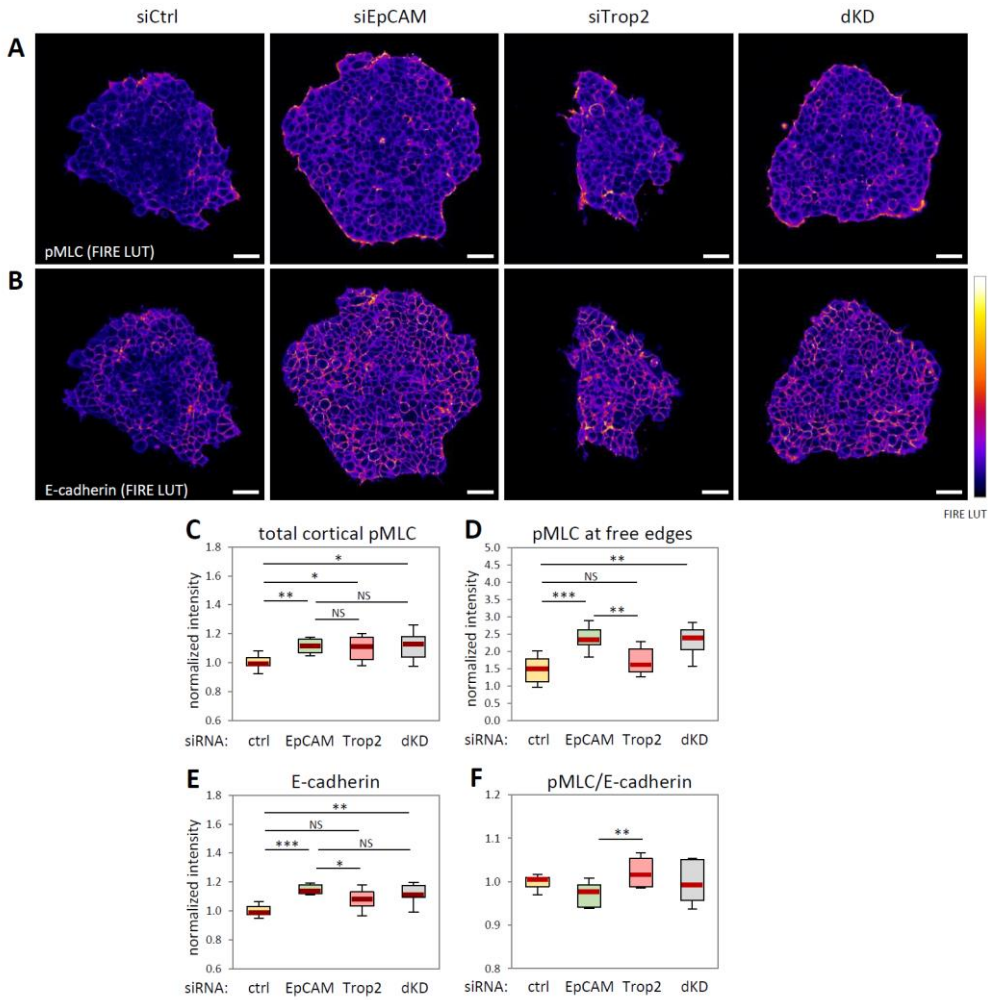

Figure 3. EpCAM and Trop2 depletions both enhance cortical myosin activation and E-cadherin recruitment at cell contacts of MCF7 spheroids. (A,B) Representative confocal images of spheroids after 24hrs spreading, immunolabelled for p-MLC and E-cadherin. Levels are visualized using the "FIRE" pseudocolors (LUT) of ImageJ. The selected z planes correspond to the widest area for each spheroid. Scale bar: 50µm. **(C-F)** Quantification of normalized mean intensities for total p-MLC (C), pMLC along the free edge of the spheroid (D), and E-cadherin (E), and calculated pMLC to E-cadherin ratio (F). Both EpCAM and Trop2 KD cause an increase in both pMLC and E-cadherin. However, the pMLC to E-cadherin ratio is lowest in EpCAM KD but highest in Trop2 KD. Eight spheroids of each condition from three independent experiments. Refer to S1 Data. One-way non-parametric ANOVA (Kruskal-Wallis) followed by Dunn post hoc test.

We characterized the properties of cell-matrix adhesion using vinculin, a classical marker of focal adhesions (FAs). Vinculin is recruited in a mechanosensitive manner, and its levels provide a readout for tension exerted on FAs. We first performed the analysis on single cells (Fig 5A). We found that the integrated FA signal per cell was increased for both EpCAM KD and Trop2 KD, and highest for dKD (Fig 5A,A'), consistent with the trend observed for cortical pMLC. We also calculated the normalized FA vinculin signal relative to the ventral cell surface (Fig 5A''), to account for the large differences in cell spreading of control, EpCAM and Trop2 KD

Figure 4

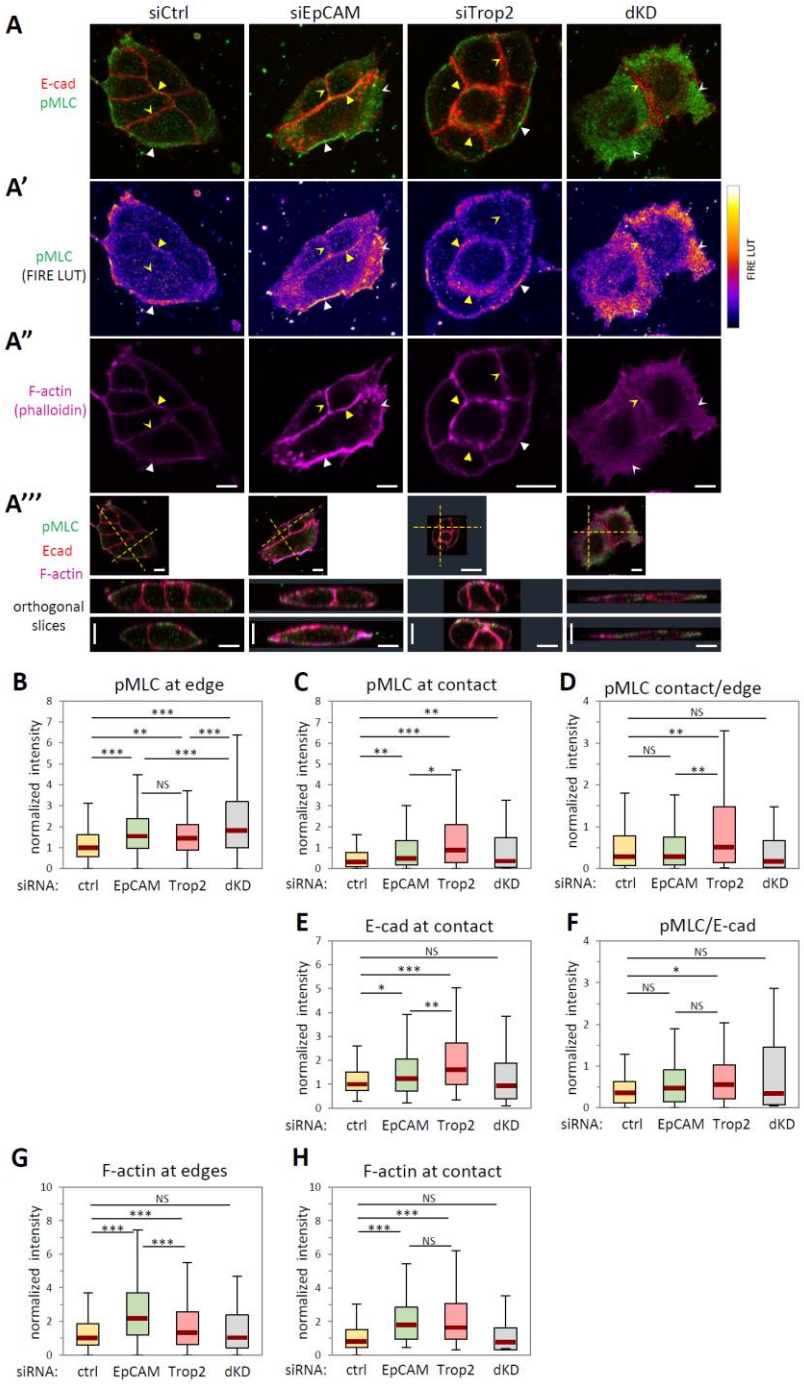

Figure 4. Impact of EpCAM and Trop2 KD on the myosin balance between cell contacts and free edges, and on E-cadherin levels in small cell groups. (A) Representative confocal images of small groups of cells immunolabelled for E-cadherin (red) and pMLC (green), F-actin filaments labelled phalloidin-Alexa647 (A″, magenta). Each image is the maximal projection of 5 planes, for a total thickness of 1µm. **(A')** pMLC signal shown as FIRE LUT. Note that the image for siTrop2 is a slightly different plane as in A, to better show pMLC at contacts. White filled arrowheads: Signal along the edge. Filled yellow arrowheads: Signal at cell contacts. Concave yellow arrowheads: Contacts with low to no pMLC signal. Concave white arrowheads: In very flat cells, the cortical signal is seen from the top (one edge of siEpCAM and the whole dKD pair). **(A''')** Comparison of size and shape through profile views (orthogonal slices along the dashed lines). Scale bars, horizontal and vertical: 10µm. **(B-H) Quantifications.** Quantification of peak intensities, determined through complete z stack series, for p-MLC along free cell edges (B) and cell-cell contacts (C), E-cadherin at contacts (D), F-actin at edges (G) and contacts (H), and calculated ratio for pMLC between contacts and free edges (D) and pMLC/E-cadherin ratio at contacts (F). pMLC and phalloidin intensities were normalized to the median value at edges of control cells. E-cadherin signal was normalized to control contacts. Data from seven independent experiments (~80-180 cells/condition). Refer to S1 Data. One-way non-parametric ANOVA (Kruskal-Wallis Test) followed by Dunn's post hoc test.

cells (Fig 5A). The results were striking: The normalized signal in EpCAM KD cells was similar to controls, while it was significantly stronger in Trop2 KD (Fig 5A"). This indicated that upon EpCAM depletion, FA strengthening and cell spreading balanced each other, while in the case of Trop2 KD, tension on the substrate was proportionally more acute. Note that despite their large area, dKD cells also showed significantly higher vinculin, indicating that tension to the matrix was exacerbated upon double depletion.

The cell/tissue interface in contact with fibrillar collagen was generally convex, presumably as the result of cells pulling on the soft substrate. This was not only obvious for spheroids (Fig 1H', S5B Fig), but also for small groups of cells (Fig 4A'''). While FAs could be segmented for single cells, this could not be done with sufficient accuracy for groups. In order to extend vinculin analysis to multicellular ensembles, we resorted to seed cells on a thinner layer of collagen (~ 5µm), on which they grew as a flat layer, allowing clear detection of FAs on a single horizontal plane (Fig 5B, and S6 Fig). As expected, here cells appeared to sense the rigidity of the underlying glass, as indicated by the abundance of strong ventral stress fibers (S6 Fig) and the intensity of the vinculin signal at FAs (Fig 5B, lower panels). This signal was significantly increased by Trop2 depletion, but not EpCAM depletion (Fig 5B'), similar to what was observed for single cells.

Vinculin is also known to be recruited in a tension-dependent manner at the cadherin-catenin complex [47], and can therefore yield information on local tension at cell-cell adhesion sites. In control MCF7 cells, we observed that vinculin did localize to some of the cell contacts, but the signal was heterogenous and generally weak (Fig 5B, higher panels, quantification Fig 5B"). Contacts of EpCAM-depleted cells showed weak vinculin, similar to controls. On the contrary, vinculin strongly accumulated at contacts of Trop2-depleted cells and, to a milder degree, in double KD cells (Fig 5B, B").

Taken together, the analyses of pMLC, E-cadherin and vinculin indicated that while depletion of either EpCAM or Trop2 boosted myosin activation at the cortex, there were key differences in their impact on cell-cell and cell-matrix adhesive interfaces, suggesting that relative tension at both cell-matrix and cell-cell adhesive contacts remained moderate in EpCAM depleted cells, but was higher in Trop2 depleted cells.

Cell-substrate and cell-cell forces are elevated upon EpCAM and Trop2 depletion

These observations prompted us to measure the actual forces exerted on these different structures. We used cell doublets, the simplest system that includes a cell-cell adhesive contact. In a first approach, we used traction force microscopy (TFM) on cell pairs adhering to H micropatterns (Fig 6A). This method had unique advantages for our purpose: The H patterns constrained the cell pair to adopt a stable configuration, providing a robust system to directly measure traction exerted on the matrix and, at the same time, to indirectly calculate the force at the cell-cell contact, simply based on the balance of forces (Fig 6A') [48]. Note that in these settings, traction exerted on the matrix appears to be similar for single cells and for cell doublets [49]. A bonus from this technique was that the H pattern, by imposing a fixed geometry and a limited surface for the contacts to the matrix, partly solved a major challenge, i.e. the wide differences in cell morphology of cells on non-constrained collagen substrate, naturally observed within the wild type MCF7 cell population, and further exacerbated by EpCAM and Trop2 depletions. EpCAM KD caused a significant increase of the total contractile energy, reflecting a strong traction exerted on the FA (Fig 6C,D). These results directly demonstrated the increased contractility in EpCAM KD cells, confirming the pMLC IF data. The global force exerted on the cell-cell contact, Fcc, was also increased, an expected result of high global cell contractility (Fig 6E). Yet, the length of cell-cell contacts, which is a readout of adhesiveness (see below), was significantly broader for EpCAM KD pairs (Fig 6B,G). This result was again consistent with EpCAM-depleted cells responding to increased contractility by cadherin recruitment and reinforcement of cell-cell adhesion. Trop2 KD also increased both total contractile energy and cell-cell forces (Fig 6C,D,E). However, contact length was only marginally increased (Fig 6B,G), supporting, together with the IF data, the notion that, while both EpCAM and Trop2 depletions upregulate myosin-dependent cortical tension, adhesion reinforcement in Trop2 KD cells was less efficient. As expected, double depletion also increased contractile energy, yielding the highest cell-cell force and highest cell-cell to total force ratio, consistent with EpCAM and Trop2 both contributing to moderating myosin contractility in these cells (Fig 6E,F).

Figure 5

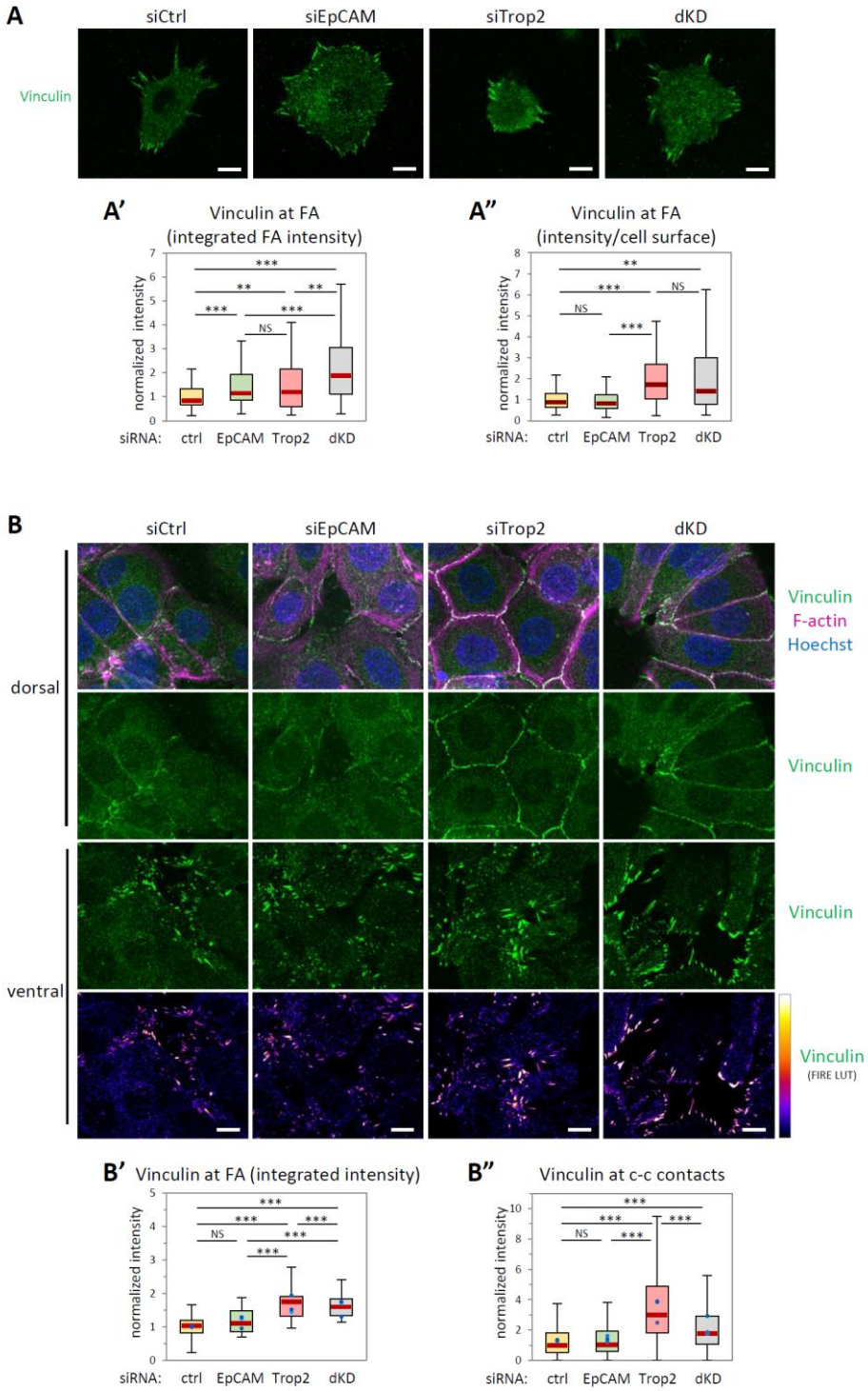

Figure 5. Trop2 KD causes a stronger recruitment of vinculin at focal adhesions and cell-cell contacts. (A) Confocal images of the ventral side (maximal projections) of single cells on collagen gel, immunolabelled for vinculin. **(A')** Quantification of integrated vinculin focal adhesion intensity, normalized relative to the median value of control cells. **(A")** Vinculin signal normalized to cell area. Data from (six experiments (~80 cells/condition). **(B)** Confocal images of large groups of cells laid on thin fibrillar collagen (~5µm thick), immunolabelled for vinculin and stained with phalloidin. Maximal projections of deconvoluted images from z stacks, 1µm slices for the ventral side, ~3µm slices for the dorsal side. **(B')** Vinculin intensity at focal adhesions, three experiments (18-20 fields/condition) for groups. **(B")** Vinculin intensity along cell-cell contacts, three experiments (~300 contacts/condition). Dots indicate medians of each experiment. Refer to S1 Data. A',A",B'B": One-way non-parametric ANOVA (Kruskal-Wallis Test) followed by Dunn's post hoc test. Scale bars: 10 µm.

Figure 6

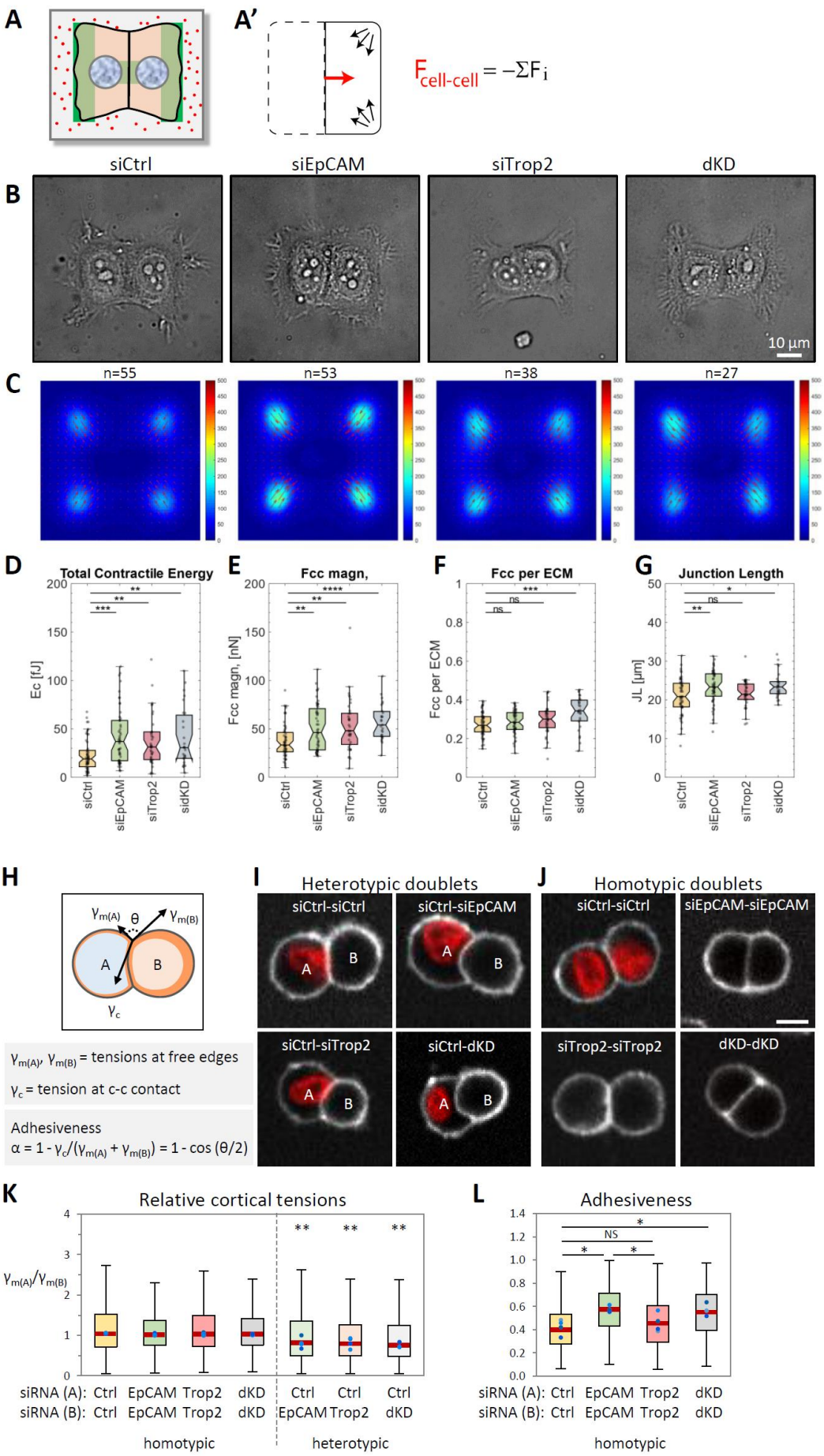
A
A'
$F_{cell-cell} = -\Sigma F_i$
B
siCtrl
siEpCAM
siTrop2
dKD
10 µm
C
n=55
n=53
n=38
n=27
D
Total Contractile Energy
Ec [fJ]
E
Fcc magn,
Fcc magn, [nN]
F
Fcc per ECM
G
Junction Length
JL [µm]
siCtrl
siEpCAM
siTrop2
sidKD
H
$\gamma_{m(A)}$, $\gamma_{m(B)}$ = tensions at free edges
γ_c = tension at c-c contact
Adhesiveness
$\alpha = 1 - \gamma_c/(\gamma_{m(A)} + \gamma_{m(B)}) = 1 - \cos(\theta/2)$
I
Heterotypic doublets
siCtrl-siCtrl
siCtrl-siEpCAM
siCtrl-siTrop2
siCtrl-dKD
J
Homotypic doublets
siCtrl-siCtrl
siEpCAM-siEpCAM
siTrop2-siTrop2
dKD-dKD
K
Relative cortical tensions
$\gamma_{m(A)}/\gamma_{m(B)}$
siRNA (A): Ctrl EpCAM Trop2 dKD Ctrl Ctrl Ctrl
siRNA (B): Ctrl EpCAM Trop2 dKD EpCAM Trop2 dKD
homotypic
heterotypic
L
Adhesiveness
NS
siRNA (A): Ctrl EpCAM Trop2 dKD
siRNA (B): Ctrl EpCAM Trop2 dKD
homotypic

Figure 6. EpCAM KD and Trop2 KD differentially increase traction on the substrate, cortical tension, and cell-cell adhesion. (A-D) Traction Force Microscopy (TFM) of cell doublets on H patterns. (A) Scheme of the experimental settings. Cells doublets were laid on H patterns coated with a thin layer of collagen (green) on a polyacrylamide gel with a stiffness of 5kPa, containing far red fluorescence nanobeads. Cells and underneath nanobeads were imaged, then cells were removed by trypsinization, and second images of the same positions were taken and used as reference, from which bead displacement was measured. **(A')** Diagram of force vectors obtained by TFM on H-shape micropatterns. While traction forces (black arrows) are measured from the displacement of nanobeads, the cell-cell force (red arrow) is calculated indirectly based on it counterbalancing the sum of traction forces, as shown in the equation. **(B)** Representative images of micropattern-confined cell doublets for the four experimental conditions. **(C)** Corresponding average maps of traction forces. **(D)** Quantification of traction forces. **(E)** Quantification of cell-cell forces. **(F)** Cell-cell force to traction force ratio. **(G)** Quantification of junction lengths, measured from the phase contrast images. One-way ANOVA followed by Tukey-HSD post-hoc test. **(H-L) Determination of relative cortical tension and cell-cell adhesiveness of cell doublets laid on a non-adhering surface. (H)** Diagram of an asymmetric cell doublet, with the balance between cortical tensions at the free edges ($\gamma_{m(A)}$ and $\gamma_{m(B)}$) and contact tension ($\gamma_{c(AB)}$) as introduced in Box 1. The principles of such system are as follows: The directions of the force vectors $\gamma_{m(A)}$, $\gamma_{m(A)}$ and $\gamma_{c(AB)}$ are tangential to the membranes at the cell vertex, which allows to directly calculate the relative strengths of these tensions based on the geometry at vertices. The orange layer represents the actomyosin cortex, with its thickness symbolizing relative contractility. In the configuration represented in the diagram, the curved cell-cell interface reflects differences in cortical tension, as cell A tends to partly engulf B, due to its lower tension ($\gamma_{m(A)} < \gamma_{m(B)}$). The strength of adhesion is related to the capacity of downregulating cortical tension along the cell-cell contact (Box 1). θ, the angle formed by the two vectors $\gamma_{m(A)}$ and $\gamma_{m(B)}$, directly relates to adhesiveness, a dimensionless value that ranges from 0 to 1. **(I,J)** Examples of homotypic and heterotypic doublets imaged by live confocal microscopy. The doublets were formed by mixing dissociated cells and let them re-associate on an adhesion-free support. Membranes were labeled with CellMask Alexa Fluor 647. siCtrl (A) cells were marked by Hoechst staining (showed in red) prior dissociation. Scale bar: 10µm. **(K)** Quantification of relative cortical tensions expressed as the ratio $\gamma_{m(A)}/\gamma_{m(B)}$. As expected, under all conditions, the ratio is close to 1 for homotypic doublets. The ratio for heterotypic doublets is significantly lower, demonstrating that single and double depletions all cause an increase in cortical tension. **(L)** Quantification of adhesiveness for homotypic doublets, calculated from γ_c and γ_m. Values show that EpCAM KD or dKD cells have increased adhesiveness compared to control cells. Trop2 KD only leads to a weak, non-significant increase. Four independent experiments, total 500-1250 doublets. Experiment averages indicated by dots. One-way non-parametric ANOVA (Kruskal-Wallis Test) followed by Dunn post-hoc test on experimental averages.

The substrate used for TFM was an acrylamide gel coated with collagen. We verified the effect of EpCAM KD on spreading of spheroids on this acrylamide-based substrate. We found essentially the same phenotypes as on fibrillar collagen gel: EpCAM depletion strongly increased spreading, while maintaining high cohesiveness as indicated by high solidity values (S7 Fig).

EpCAM KD modulates cortical tension and adhesiveness in substrate-free cell doublets Our TFM data provided a simultaneous quantitative measurement of cell-matrix and cell-cell adhesion. The next assay was aimed at evaluate relative cortical tension at free edges and cell-cell contact interface, and providing a clean measurement of cell-cell adhesiveness in the absence of any other interactions. These parameters can be accurately measured simply based on the geometry of free cell doublets laid on a non-adherent surface [43,46,50–52]. Such doublets adopt a typical configuration, where the cell contact expands until contact tension γ_c, ($\gamma_{c(AB)}$ in the diagram of Fig 6H) is precisely balanced by the cortical tension at the interface with the medium γ_m). Furthermore, if the two cells differ in their cortical tensions ($\gamma_{m(A)}$ and $\gamma_{m(B)}$, Fig 6H), the doublet adopts an asymmetric geometry, as the softer cell tends to engulf the stiffer cell (Fig 6H). The relative value for the three tensions, $\gamma_{m(A)}$, $\gamma_{m(B)}$ and $\gamma_{c(AB)}$ can be directly deduced from the geometry of the membranes at the contact vertex [46,50,52,53]. From these measurements, two important information can be extracted: a) The relative cortical tensions γ_m of the two cells, expressed as $\gamma_{m(A)}/\gamma_{m(B)}$, and b) the $\gamma_{c(AB)}/\gamma_{m(A)}$ ratio, which directly reflects the state of adhesion of a contact. A convenient way to express this relationship is "adhesiveness" [46], an absolute number between 0 and 1, which is inversely related to the γ_c/γ_m ratio (Fig 6L) and positively related to contact length as well as to the angle θ (Fig 6H).

We adapted the protocol previously used for embryonic cells [50,53,54] to mildly dissociate MCF7 monolayers into single cells, which we mixed at low density two populations to favour formation of both homotypic and heterotypic doublets, which we imaged by confocal microscopy (Fig 6I,J). We systematically analyzed the effect of single and double EpCAM and Trop2 KD cells and made the following observations. Firstly, heterotypic doublets made of a control (A) and a depleted cell (B) were clearly asymmetric (Fig 6I), corresponding to a

Figure 7

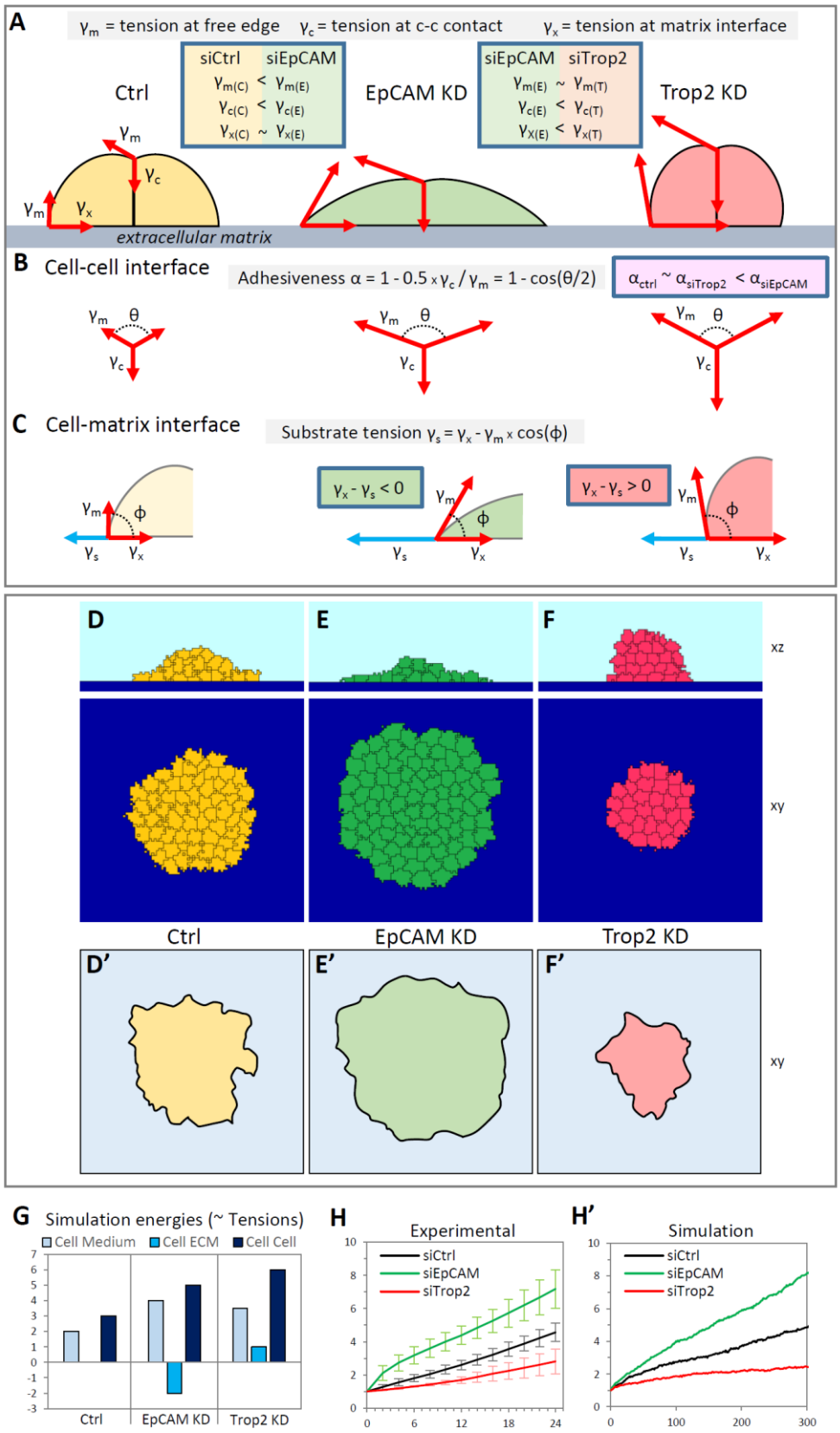

Figure 7. Simulation of MCF7 spheroid spreading in controls and under EpCAM/Trop2-depleted conditions based on biophysical parameters. A. Representation of schematic cell doublets on a substrate, with the relative tension vectors represented at the cell-cell vertex and at the edge of the matrix substrate interface. Their relative strength is represented by the length of the vector. The general changes in tensions between control and EpCAM KD, and between EpCAM KD and Trop2 KD are summarized in the two boxes with blue borders. **B**. Balance of forces at the cell-cell vertex. While all three tensions are strongly increased both in EpCAM KD and Trop2 KD, the resulting adhesiveness,

which can be directly deduced from the angle θ, is increased in EpCAM KD but not in Trop2 KD. **C**. Balance of forces at the matrix interface. γ_s is the tension exerted on the substrate, corresponding to the traction measured by TFM. It counterbalances the cell-matrix tension γ_x and the horizontal component of the cell-medium tension γ_m. Both tensions are increased in EpCAM and Trop2 KD, but their relative balance determines different outcomes: EpCAM KD cells adopts a spread configuration (acute angle φ), while, on the contrary, Trop2 KD cells have a compact shape (obtuse angle φ). For simplicity, only the horizontal component of the substrate tension is represented. **D-F.** Simulation of spheroids spreading using a 3D cellular Potts model (CompuCell3D software) for control, EpCAM KD and Trop2 KD conditions. See annex for detailed information. Images correspond to examples of yx and yz planes after 300 iterations. Medium is in light blue, matrix substrate in dark blue. **D′-D′.** Outlines of explants at 24hrs from Fig 1, drawn for comparison. **G.** Energy parameters used to simulate the three conditions. **H,H′.** Comparison of curves of relative area expansion from experimental data and from simulation. Error bars: SD. Refer to S1 Data.

ratio between the two cortical tensions γm(A)/γm(B) significantly lower than 1. This constituted a firm demonstration that cortical contractility was indeed increased upon EpCAM and Trop2 KD (Fig 6K). Second, contact angles of homotypic doublets were less acute for EpCAM KD than controls (Fig 6J), corresponding to a significant increase in adhesiveness (median 0.58 compared to 0.40 for controls (Fig 6L). In the case of Trop2 KD, however, only a small, non-significant increase was observed (Fig 6L). dKD doublets were similar to EpCAM KD (Fig 6L). These two results were in perfect agreement with IF and TFM data, demonstrating that while both KD led to increased contractility, only EpCAM KD efficiently boosted adhesiveness.

Spheroid spreading phenotypes can be simulated based on cell tensile properties

We asked whether our characterization of contractile and adhesive properties could account for the striking differences in the behaviour of the spheroids. Based on the principles enunciated in Box1, a simple description of the experimental conditions can be made based on balance of the tensions exerted along the three cell interfaces γ_m, γ_c, and γ_x. As mentioned above, the relative strengths of γ_c and of γ_m determine adhesiveness α (Fig 6H, 7A-C). One key observation was that EpCAM KD cells had higher adhesiveness than control cells (Fig 6G,L), despite being more contractile (Fig 6D,K). This effect was explained by the stronger increase in γ_m relative to γ_c (Fig 7A,B). In the case of Trop2 KD cells, both γ_m and γ_c were also increased, but their relative values were roughly maintained, without significantly changing adhesiveness (Fig 6G,L and Fig 7B). Spreading on the extracellular matrix can be similarly described based on γ_m and γ_x, which are counterbalanced by the tension of the elastic substrate γ_s (for simplification, we consider here only the horizontal component) (Fig 7C). This balance of force can be expressed as $\gamma_s = \gamma_x - \gamma_m * \cos(\Phi)$. As consequence of this relationship, if $\gamma_s = \gamma_x$, the edge of the cell forms a right angle with the substrate. For $\gamma_s - \gamma_x < 0$, the cell spreads more on the substrate, forming an acute angle Φ, while on the contrary, for $\gamma_s - \gamma_x > 0$, Φ is obtuse, thus the cell tends to contract. These three situations corresponded to the conditions that were used in our experiments, respectively controls, EpCAM KD and Trop2 KD (Fig 7A,C). The correspondence was supported by the comparison between γ_s and the total contractile energies from TFM (Fig 6D), by the xz projections of the single cells (Fig 2F,G), and by the vinculin data (Fig 5), which were qualitatively consistent with relative γ_x values. It is essential here to note that the extent of spreading of a cell on the substrate ("wetting") does not depend on absolute tension strengths, but on their relative values. Thus, while γ_m, γ_x and γ_s were all increased in both EpCAM KD and Trop2 KD, the γ_x to γ_m ratio changed in opposite directions, causing EpCAM KD cells to be flatter, and Trop2 KD to be taller.

With these cellular parameters at hands, we thought to simulate spheroid spreading using a cellular Potts model [55,56], specifically a 3D version (CompuCell3D [57,58]). In this model, the "tensions" for a given cell type are input as relative "energies" (see appendix). While these energies are arbitrary values, they are related to γ_m for the cell-medium energy, γ_c for cell-cell energy, and γ_x-γ_s for cell-matrix energy. We considered an initially compact group of cells laid on a flat surface, and set the three energies (Fig 7G) to fit our data on single cells and cell doublets (Fig 2F,G and S8 Fig and annex, qualitative summary Fig 7A-C). The key features were (1) higher global energy for both EpCAM KD and Trop2 KD, which accounted for increased contractility compared to controls, nuanced by specific differences between the two depletions, (2) a lower cell-cell energy/cell-medium energy ratio (thus higher adhesiveness) for EpCAM KD, as well as (3) a cell-substrate energy set negatively for EpCAM KD, and positively for Trop2 KD, consistent with their respective spreading and contracting properties. Simulation of the behaviour of spheroids under these three conditions yielded clear

differences in the degree of spreading, moderate for the control condition, high for EpCAM KD, and very low for Trop2 KD (Fig 7D-F, H, Movies 9 and 10), which faithfully reproduced the experimental spheroid spreading phenotypes (Fig 7D'-F', H'). Note that we purposely chose to perform simulations that only considered the three cellular tensions. Indeed, the goal was to highlight the explanatory power of this simple model that could recapitulate very well the spreading phenotypes. The simulations did not fully mimic more detailed aspects of the spheroid morphology, in particular the convoluted outlines of the Trop2 KD spheroids (Fig 7F,F'), which would require to complexify the model with additional parameters, e.g. properties of protrusions. In summary, we show here that the experimentally observed differences in cortical contractility at different interfaces are sufficient to account for the diametrically opposite spreading behaviours produced by EpCAM and Trop2 depletions.

Partial differential subcellular distribution of EpCAM and Trop2 may account for the distinct phenotypes

A simple possible explanation for the opposite phenotypes could be differences in distribution of the two regulators, which may then preferentially act on one or the other of the cell interfaces. We set up to determine these distributions by quantitative IF on small groups of cells (Fig 8 and S9 Fig). Consistent with their global impact on contractility and adhesiveness, EpCAM and Trop2 were both strongly expressed all along the plasma membrane, including cell-cell contacts. Standard IF with post-fixation permeabilization detected few EpCAM and/or Trop2-positive intracellular spots, that represented a negligible pool relative to the surface signal (S9E Fig). Because permeabilization led to a significant loss of Trop2 signal at the plasma membrane, we present data from cell surface labelling without permeabilization, which gave robust signals for both proteins (Fig 8A). We quantified their distribution along specific plasma membrane regions, namely the ventral side in contact with the cell-matrix, the cell-cell contacts, as well as the surface exposed to the medium, i.e. the dorsal side and lateral free edge, excluding protrusions that were measured separately (diagrams Fig 8B' and S9A Fig). These main locations corresponded to the sites where the three basic cortical tensions are exerted, respectively γ_x at the ventral matrix interface, γ_c at cell-cell contacts, and γ_m on the dorsal and lateral sides. Additional subregions were defined for a more detailed analysis (S9A-C Fig). The two molecules showed a very similar distribution, with close to identical relative levels in most locations (S9B Fig). However, we found a conspicuous difference between the free interface (dorsal side and lateral edges) and the ventral side, the latter containing significantly more Trop2 than EpCAM (Fig 8B, S9B Fig). The resulting difference in dorsal/ventral ratio was modest (~20%) but highly reproducible (Fig 8C). A second striking difference was measured for cell-cell contacts, specifically for contacts at the interior of cell groups (here named inner contacts), where Trop2 was also enriched relative to EpCAM (Fig 8D-F, S9D Fig). These observations prompted us to go back to EpCAM and Trop2 IF images of whole spheroids. Bearing in mind that here detergent permeabilization was required, with the caveat of partial loss of Trop2 signal, the general trend was consistent, with Trop2 signal prominently low at the edges of the spheroids, and brightest along internal contacts (S10 Fig).

In summary, while EpCAM and Trop2 broadly distributed at all cell interfaces in wild type MCF7 cells, relative enrichments were found at key location, with EpCAM being proportionally higher at free edges, Trop2 higher at the matrix interface, as well as at cell-cell contacts. although in the latter case, levels varied in the various subdomains (Fig 8, S9B Fig), and should be further mapped in greater detail. These distributions and the potential link with cortical tensions are graphically summarized in the diagrams of Figure 8I. In the simplest model, the distribution of tensions in EpCAM or Trop KD could in principle be predicted by subtracting the myosin-inhibitory contribution of the depleted molecule. In particular, the dorsal/ventral and edge/contact asymmetries could readily explain why Trop2 depletion led to a comparatively stronger increase in tension along contact interfaces (Fig 8I).

However, wild type distribution alone was not sufficient to safely predict the impact of these depletions on the three cortical tensions. It was essential to determine whether EpCAM and Trop2 were sensitive to the loss of the other protein. The results of this analysis are presented in Fig 8G,H and S9C Fig, and summarized in Fig 8I. EpCAM levels and distribution were largely unaffected in Trop2 KD cells. The situation was different for Trop2, which was significantly impacted by EpCAM KD: Its levels decreased on the whole lateral and dorsal

Figure 8

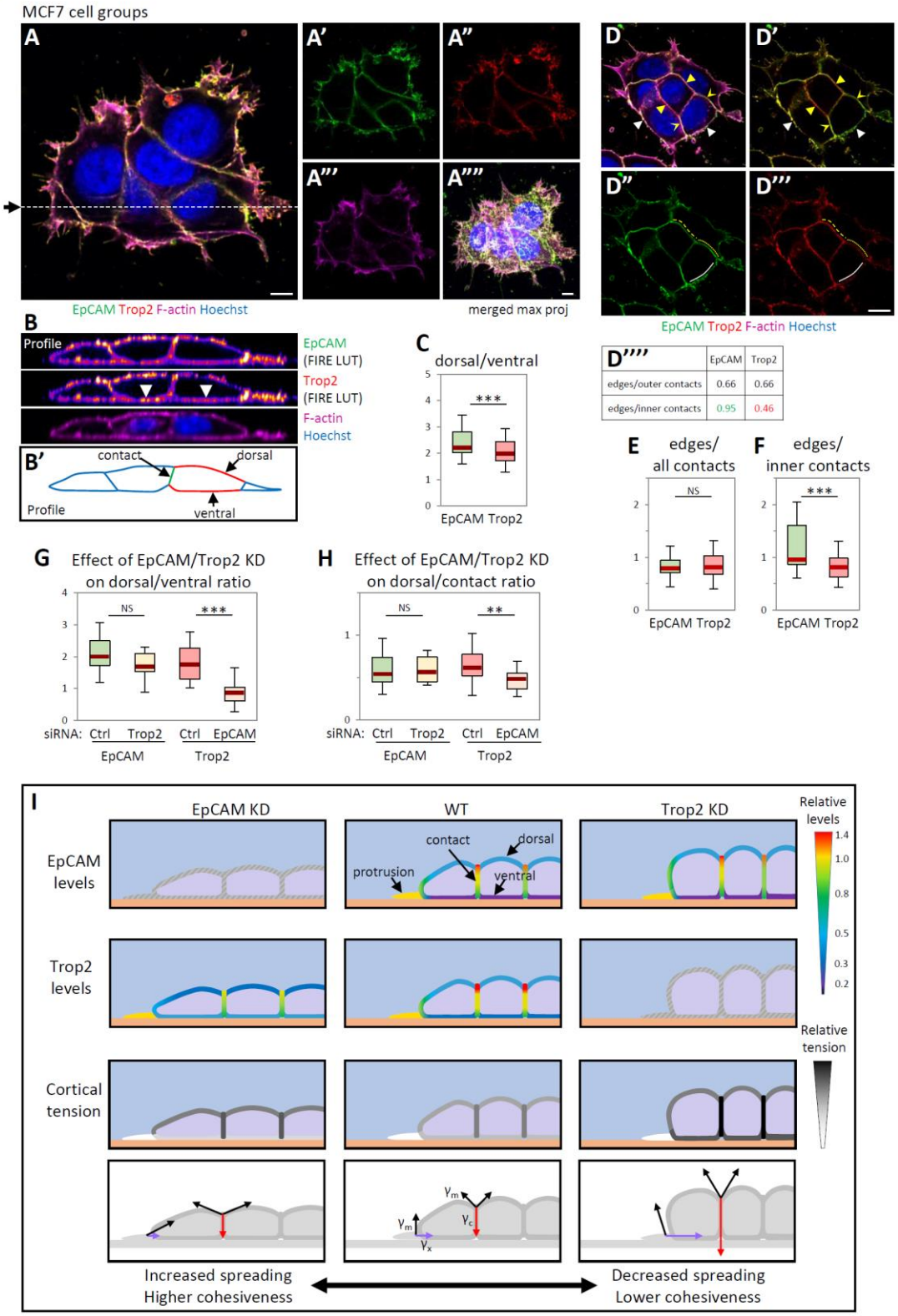

Figure 8. EpCAM and Trop2 differential distribution along cell interfaces of MCF7 cells and impact of depletions. **(A-B)** Confocal microscopy image of a small group of wild type MCF7 cells on collagen gel, labelled under non-permeabilized conditions for EpCAM (green), Trop2 (red) and F-actin (phalloidin-Alexa647, magenta). EpCAM and Trop2 levels where analyzed from whole z-stacks, as well from resliced stacks to obtain profile projections (see details in S9 Fig). Both EpCAM and Trop2 were found distributed all along the plasma membrane, but there was a partial but reproducible difference between the free edges (dorsal and lateral), richer in EpCAM, and the ventral side, richer in Trop2. **(A)** Horizontal plane, merged image. **(A',A'',A''')** Individual channels. **(A'''')** Maximal projection of the whole stack. **(B)** Profile view of the same group. The position of the orthogonal slice is indicated by the white dashed line in A. EpCAM and Trop2 channels are displayed as "FIRE" LUT. The patterns of the two regulators appear virtually

identical, except for slightly higher Trop2 levels at the ventral side (arrowheads). **(B′)** Diagram of the three main interfaces quantified based on profiles. See S9 Fig for complete diagrams of horizontal and profile regions (12 categories) and corresponding full quantitative analysis. **(C)** Pairwise quantification of dorsal and ventral levels for EpCAM and Trop2 show that the ratio is significantly lower for Trop2. Data from 14 groups, 3 experiments. Refer to S1 Data. **(D)** Example of cell group with a central cell, surrounded by "inner" contacts (D,D′, yellow arrowheads; D″,D‴ dashed yellow line). As obvious in the merge of panel D′, these contacts have proportionally lower EpCAM/higher Trop2 compared to outer contacts (yellow concave arrowheads and yellow dotted line) and free edges (white arrowheads and white dotted line). **(D‴′)** Ratios edges/outer contacts and edges/inner contacts for this particular group. **(E,F)** Quantification of 24 groups of 6-12 cells, from 5 experiments, of which 14 groups had inner contacts. (E) Ratio edges to all contacts of a group, for EpCAM and Trop2. (F) Ratio edges/inner contacts, significantly higher for EpCAM. Trop2 relative enrichment in inner contacts was also systematically observed in larger groups (example in S9F Fig). Refer to S1 Data. Statistical analysis: Pairwise Student's t-test. Scale bars: A, 5µm; D, 10µm. **(G-H) EpCAM depletion influences Trop2 distribution, while EpCAM is not impacted by Trop2 depletion.** Dorsal/ventral ratio (G) and dorsal/cell-cell contact ratio (H) were calculated for control, siEpCAM and siTrop2 cell groups. See details of relative levels in S9C Fig). Results from 13-14 cell groups, 3 experiments. Refer to S1 Data. Statistical analysis: Pairwise Student's t-test. **(I) Summary diagram of EpCAM and Trop2 distribution in wild type and depleted MCF7, and impact on cortical tensions.** The schemes represent three cells at the edge of a migrating group. The major regions are drawn, including dorsal, lateral and ventral surfaces, cell-cell contacts, and a leading edge lamellipodium. The collagen matrix is in orange. The two top rows of panels use a colour code to recapitulate the relative levels of EpCAM and of Trop2 under wild type and EpCAM/Trop2-depleted conditions. The third row provides a summary of cortical tension at the various interfaces using an arbitrary grey scale. The lower row represents the three corresponding cellular tensions γ_m (black), γ_c (red), and γ_x (purple).

free edges, while it was increased at the ventral interface (S9C Fig). This resulted in a significant shift in the dorsal/ventral and dorsal/cell contact ratios (Fig 8G). These changes were of importance for interpreting the EpCAM KD phenotypes, since they were bound to exacerbate the tension imbalance caused by EpCAM loss, further increasing edge tension γ_m and decreasing contact tensions γ_x and γ_c, thus boosting spreading on the matrix as well as tissue cohesion. Note that protrusions were strongly positive for both proteins, which might account for maintaining protrusive activity even in depleted cells.

In summary, EpCAM and Trop2 had a similarly broad distribution in wild type cells, and well likely to contribute in a similar manner to moderate global cortical contractility. Yet, partial asymmetries, further amplified in the case of EpCAM KD, could account for the changes in interfacial tensions estimated experimentally (Fig 6) and inputted in our simulations (Fig 7). The resulting tension imbalances could in turn explain the surprisingly opposite phenotypic outcomes in terms of spreading and collective migration.

Differences in polarization may account for differences in single cell migration

The effect of EpCAM and Trop2 depletions on single cell migration was not fully intuitive. In particular, the rounded morphology of Trop2 KD cells (Fig 2) and the strong vinculin enrichment at FAs (Fig 5A) were not a priori typical signs of migratory cells. Yet, one general difference that was consistent with these effects on migration was the spatial arrangement of the protrusions and of the associated FAs (S11 Fig). Cells displayed a variety of morphologies, which we compiled into five categories reflecting both the degree of spreading and symmetry/asymmetry (S11F Fig, examples provided in S11A-E Fig). Control cells displayed a wide range of spreading, but the majority of them had FAs distributed in asymmetric patterns (S11C Fig). EpCAM KD cell did not only spread quite extensively, but FAs were, in the vast majority of cases, arranged in strikingly radially symmetric patterns (S11A,B Fig). In Trop2 KD cells, even though the substrate contact interface was generally round, with FAs arranged as a peripheral ring, the symmetry was broken in most cases, either through a gap in the FA ring (S11D Fig, filled and concave arrowheads), or emission of a dominant protrusion that conferred a unipolar configuration (S11E Fig). These observations argued that highly spread cells tended to adopt a stable radial configuration, while cells with a smaller contact area were more prone to a break of symmetry that allowed effective migration.

EpCAM expression favours escape of individual cells from MCF7 spheroids

MCF7 cells are considered to display high cell-cell adhesion and low migration, characteristic of epithelial cells. Consistently, spheroids spread as a compact cell mass. Yet, a close look at our time lapses of wild type spheroids showed occasional detachment and migration of individual cells (Fig 9A, Movie 11). We found that 25 out of 84 control spheroids (from 13 experiments) had at least one isolated cell that detached and migrated away over

the first 24 hr of imaging, and 7 additional spheroids even showed detachment of small groups of cells (Fig 9E). EpCAM KD (Fig 9B, Movie 12) appeared to drastically repress such events (only three cases of detachment for 85 spheroids, Fig 9E). The frequency of cell detachments was higher with Trop2 KD spheroids, here cells leaving mostly as small groups (Fig 9E, a pair of cells in the example of Fig 9C and Movie 13). Detachments were rare in dKD (Fig 9D,E, Movie 14). The same phenomenon of EpCAM-dependent single cell detachment was also observed for spheroids laid on collagen-coated polyacrylamide (S7 Fig). These results indicated that EpCAM expression favoured cells breaking out of the compact cell mass. Even though these events were rare for this particular cell line under our experimental conditions, the repressive effect of EpCAM may be relevant for cancer invasion.

Figure 9

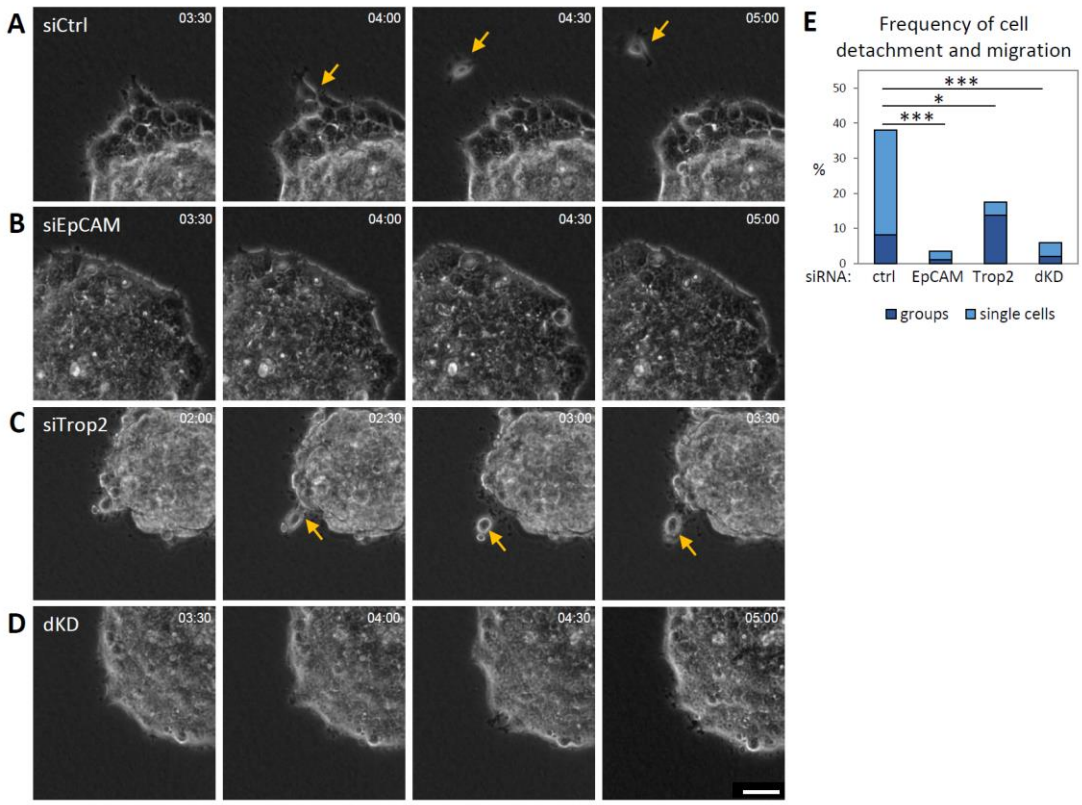

Figure 9. EpCAM depletion prevents single cell escape. (A-D) Selected time frames of time lapse movies showing edges of spheroids. Control MCF7 spheroids occasionally show single cells breaking off and migrating away (A, arrow). This almost never happens, at least within 24hrs of imaging, for siEpCAM spheroids (B), while it does occur in siTrop2 (C). **(E)** Proportion of spheroids showing at least one cell or one cell group migrating away during 24hrs. Data from 84, 85, 51 and 50 spheroids (corresponding to siCtrl, siEpCAM, siTrop2 and dKD respectively) from 12 independent experiments. Refer to S1 Data. Statistical analysis: Non-parametric ANOVA (Kruskal-Wallis Test) followed by post-hoc Dunn tests.

Differential distribution of EpCAM and Trop2 and differential LOF phenotypes in other types of breast cancer cells.

We asked whether differences in EpCAM and Trop2 activities could also be detected in other cell lines. As mentioned in the introduction, we expected EpCAM and Trop2 LOF phenotypes to be highly context-dependent, yet the underlying logic may be conserved. We selected two additional luminal breast cancer cell lines, HCC1500 and MDA-MB-453, that express both EpCAM and Trop2 (The Human Protein Atlas), but differ in their morphologies and have behaviours departing in opposite directions from MCF7 cells: When grown on collagen, HCC1500 cells spread poorly on matrix (Figs 10A and 11A), but establish extensive cell-cell contacts and form coherent aggregates (Fig 10B). On the contrary, MDA-MB-453 rapidly spread and migrate, and, while capable of cell-cell adhesion, form less extensive cell contacts (Fig 12).

Figure 10

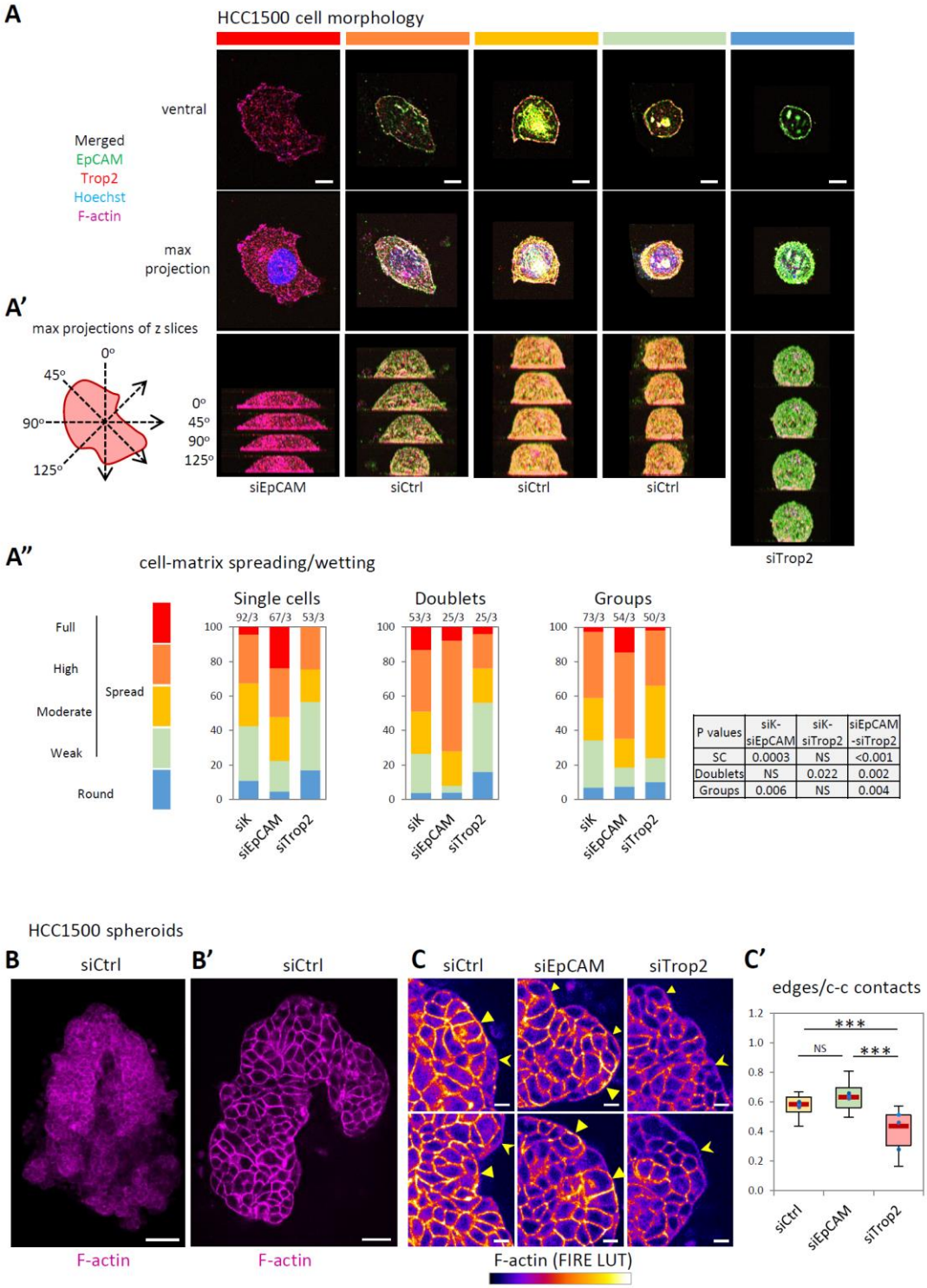

Figure 10. Opposite phenotypes of EpCAM KD and Trop2 KD in HCC1500 cells. (A) EpCAM KD and Trop2 KD differentially impact on substrate wetting. HCC1500 cells seeded on a collagen gel were immunolabelled for EpCAM and Trop2, stained with phalloidin and Hoechst, and imaged by confocal microscopy. The morphological analysis focused on the profile of the free outer margin, indicative of the degree of wetting. Because of the irregular cell and group shapes, z stacks were resliced, and orthogonal maximal projections in four orientations were produced (A'). These projections were used to classify cells cell groups, in categories of degree of spreading, from round to fully spread (A''). Intermediate categories included various combinations of partial spreading. Examples of single cells are shown in A, and groups in S11A Fig. Note that the siEpCAM condition shown here shows extreme spreading, observed for single cells but rarely for cell groups (S11A). The bar graphs show compiled results for single cells, cell doublets and groups of cells, which all show similar distributions. The table indicates p values from ANOVA analysis

followed by Tukey-HSD post-hoc test, obtained by allocating to each categories a score (0,1,2,4,6). Results were essentially the same using different scales (e.g. 0,1,2,3,4). Refer to S1 Data. Scale bars, 5 µm. **(B-C) EpCAM KD and Trop2 KD differentially impact on the cortex at free edges and cell-cell contact in HCC1500 spheroids.** Spheroids formed from control, siEpCAM and siTrop2 cells and laid on collagen gel for 3 days were stained with phalloidin and images by confocal microscopy. **(B)** Overview of a control spheroid, presented as maximal projection. HCC1500 spheroids are typically highly convoluted. **(B')** Single slice from the same spheroid. **(C)** Detailed views of spheroid edges, two examples per condition. Arrowheads point to free edges, to be compared with cell-cell contacts: Large filled, small filled and concave arrowheads indicate respectively high, moderate and low F-actin. **(C')** Quantification of the edge/contact intensity ratio. 20-24 spheroids from 3 experiments. Dots indicate averages for each experiment. Refer to S1 Data. One-way non-parametric ANOVA (Kruskal-Wallis Test) followed by Dunn post-hoc test. Scale bars: B, 100µm; B', 50µm; C, 10µm.

Figure 11

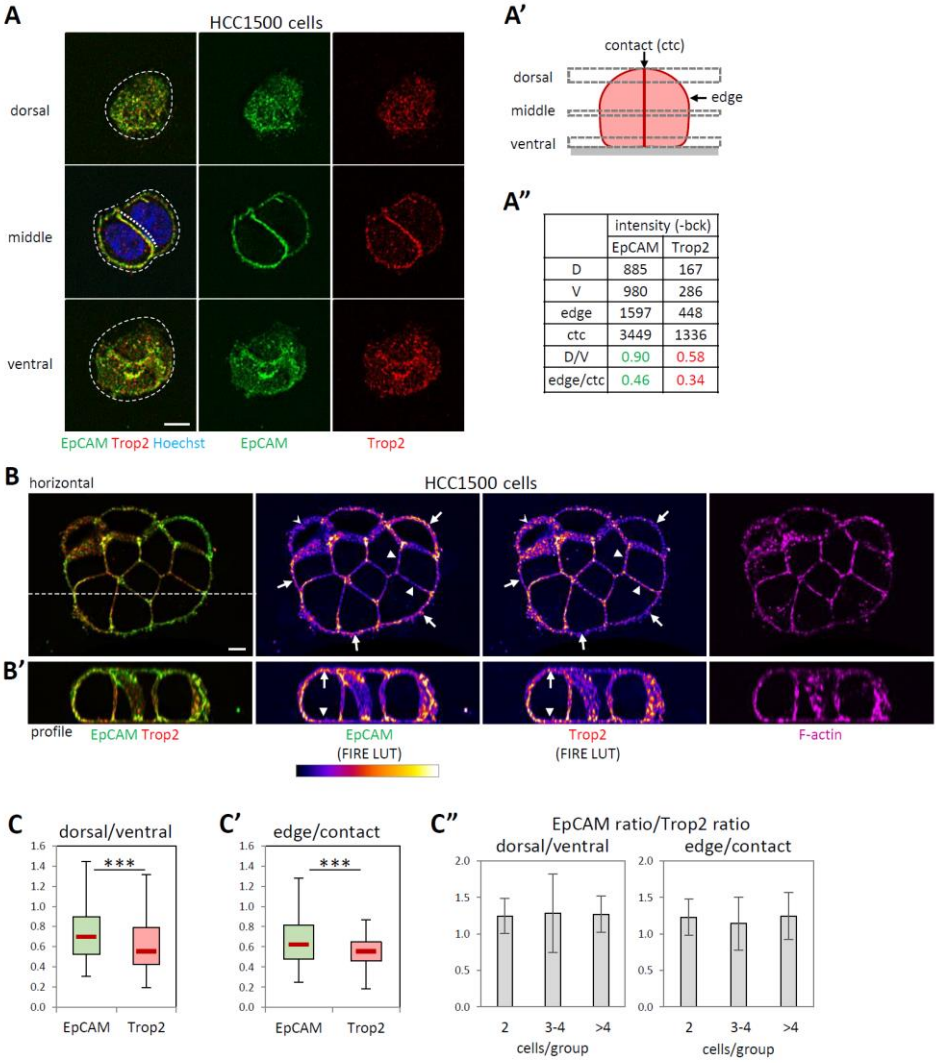

	intensity (-bck)	
	EpCAM	Trop2
D	885	167
V	980	286
edge	1597	448
ctc	3449	1336
D/V	0.90	0.58
edge/ctc	0.46	0.34

Figure 11. Differential distribution of EpCAM and Trop2 in HCC1500 cells. EpCAM levels are comparatively higher at the free edge (dorsal and lateral), Trop2 higher at cell contacts and at the ventral matrix interface. **(A)** Example of a cell doublet immunolabelled for EpCAM and Trop2, showing three slices corresponding to the dorsal (0.2µm max projection, 2 planes), middle (0.8µm max projection, 5 planes) and ventral (0.2µm max projection, 2 planes) regions (A'). Scale bar, 5µm. **(A")** Quantification for this doublet, providing average intensities, background subtracted, for dorsal and ventral surfaces, and for the lateral edge and cell-cell contact (ctc), and the resulting dorsal/ventral (D/V) and ctc/edge ratios. **(B)** Example of a group of cells labelled for EpCAM, Trop2 and F-actin (phalloidin). Arrows point to edges with higher EpCAM relative to Trop2, arrowheads to contacts with low EpCAM and higher Trop2. Small concave arrowhead: Edge with high Trop2. **(B')** Orthogonal view along the dashed line in B. Arrows point to dorsal edge, with high EpCAM, arrowhead to the ventral interface, with higher Trop2. **(C,C')** Quantification of dorsal/ventral and edge/contact ratios for EpCAM and Trop2 intensities, for groups ranging from doublets up to 20 cell-large groups. **(C")** Calculated EpCAM ratios divided by Trop2 ratios for groups of different sizes, showing that the relative enrichments are constant over the whole range. 67 groups from 3 experiments. Refer to S1 Data. Statistical analysis using Student's t-test. Scale bar: 20µm.

The morphology of HCC1500 cells laid on collagen gel, whether single or in small groups, was affected in opposite directions by EpCAM KD and Trop2 KD: Spreading was significantly stimulated by EpCAM KD, while further diminished upon Trop2 KD (Fig 10A, S12 Fig). Thus, despite the large differences in morphology and spreading capacity of MCF7 and HCC1500 cells, the effects of EpCAM and Trop2 LOF on substrate "wetting" strikingly followed the same trends. We succeeded at forming HCC1500 spheroids, but found that they adhered poorly to the matrix and did not expand (Fig 10B). EpCAM or Trop2 depletion had no detectable impact on this behaviour. However, we observed a clear effect on the cell cortices, visualized by phalloidin staining (Fig 10C). We found that the ratio between the average intensities at free edges and at cell-cell contacts changed in opposite directions, highest for EpCAM KD and lowest for Trop2 KD (Fig 10C'), again indicative of a change in the balance between the cortical regions. While further characterization of the HCC1500 phenotypes will be needed, these data are compatible with EpCAM KD decreasing the tension balance between contacts and free edges, thus increasing cell-cell adhesiveness, Trop2 KD having the inverse effect. Note that due to the highly irregular morphology of these spheroids, we could not satisfactorily segment and quantify the ventral phalloidin signal.

We analyzed the distribution of EpCAM and Trop2 in wild type HCC1500 cells (Fig 11). While the signal intensities varied from cell to cell, there was again a general trend for differential localization: The ratio between the dorsal and ventral sides was slightly but significantly higher for EpCAM than for Trop2 (Fig 11A,B, best seen in profile view B', quantification in Fig 11C). Furthermore, EpCAM signal was also proportionally higher at the lateral edges compared to the cell-cell contacts (Fig 11A and B, quantification in Fig 11C'). This asymmetry was essentially the same for all sizes of cell groups (Fig 11C"). In conclusion, EpCAM had also a preference for the free membrane region, Trop2 for the ventral surface and for cell contacts, similar to what observed in MCF7 cells.

MDA-MB-453 spheroids adhered and spread rapidly and more extensively than MCF7 spheroids, expanding as a thinner and looser layer (Fig 12A-C). Single cells frequently detached and migrated ahead, eventually being caught up by the rest of the rapidly expanding mass (S13 Fig). After 18hrs, a large portion of the cell mass had already migrated away from the original core, the remnant of which still emerged as a dome (Fig 12A,B'). The area of this dome was estimated and expressed relative to the total area of the expanded spheroid (Fig 12C,C"). EpCAM or Trop2 KD did not significantly change the area increase after 18h spreading (Fig 12A,B,C'). However, EpCAM and Trop2 depletions did lead to clearly divergent phenotypes in terms of spheroid morphology. Upon EpCAM KD, the majority of spheroids spread into a flatter disc, with the central dome less prominent (Fig 12A,B') or absent (about 1/5 of the spheroids, Fig 12C"). Enlarged profile views (Fig 12B') showed that cells near the edge maintained extensive contacts. Altogether, the EpCAM KD phenotype was consistent with higher tissue cohesion, similar to MCF7 cells. In Trop2 KD, on the contrary, the core of the spheroid remained more massive (Fig 12A,B'.C"), while a thin monolayer of cells spread on the matrix, often tenuously connected with the core, as exemplified in the profiles of Fig 12B'. In contrast to the prediction from the transcriptomic data, EpCAM and Trop2 levels in MDA-MB-453 cells were surprisingly low (Fig 12D). We could quantify dorsal and ventral signals for a subset of cells that displayed sufficiently high signal relative to background (Fig 12D), and calculate the dorsal to ventral ratios. EpCAM was clearly enriched dorsally, and Trop2 ventrally (Fig 12 E). We concluded that in all these three very different cell lines, EpCAM and Trop2 showed a consistent partial asymmetric distribution, and in all cases, their depletions led to phenotypes consistent with opposite effects on wetting and adhesiveness.

Figure 12

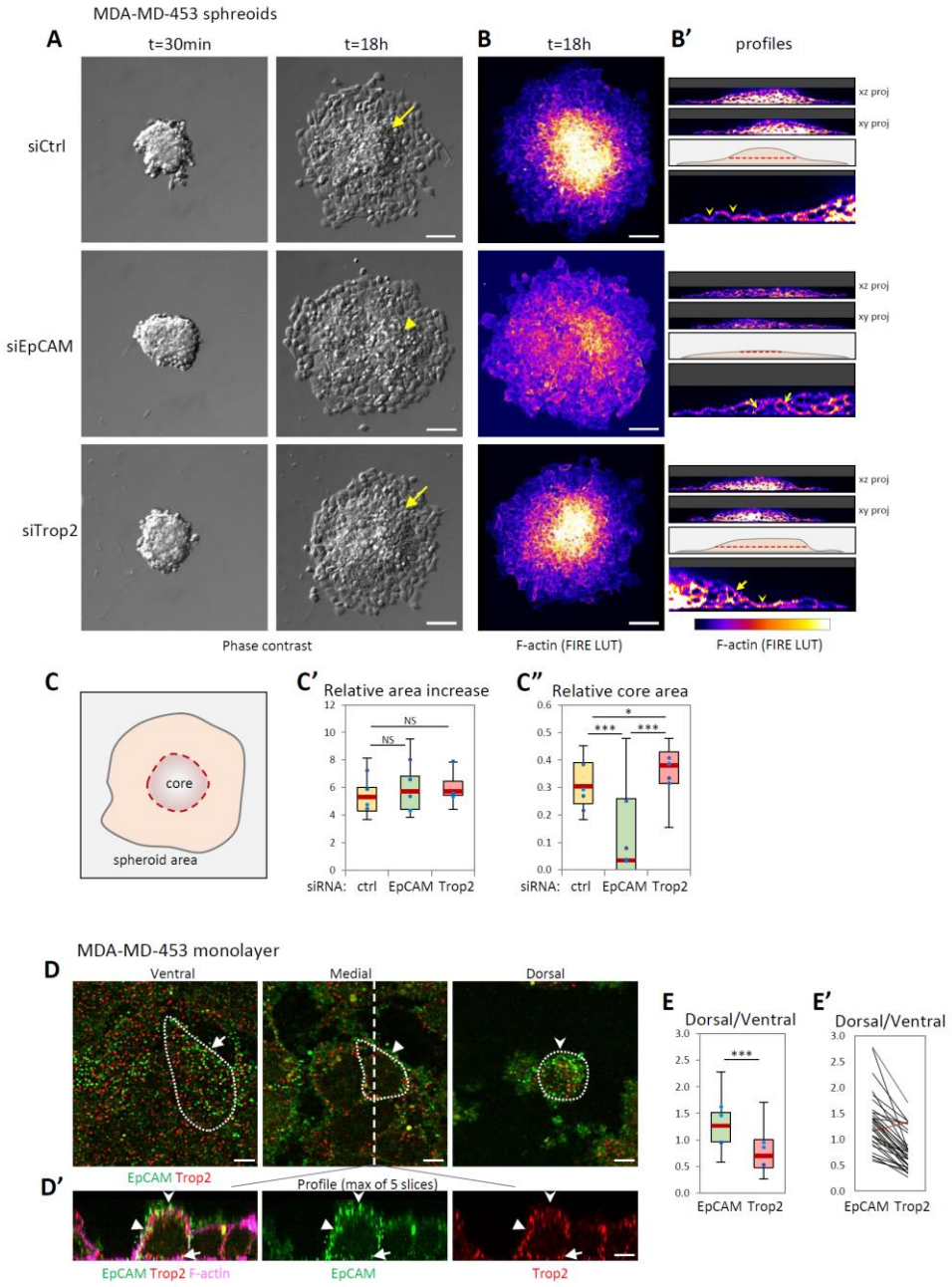

Figure 12. Differential spheroid phenotypes of EpCAM KD and Trop2 KD and differential distribution of EpCAM and Trop2 in MDA-MD-453 cells. (A) Control, EpCAM KD and Trop2 KD spheroids, shortly after adhering to the collagen gel (t=30min), and after 18hrs. Spheroids have extensively spread. In control spheroids, a remnant core of the original cell mass can still be seen as a dome (arrow). In EpCAM KD spheroids, the dome is much smaller (arrowhead) and often absent. In Trop2 KD spheroids, the core is typically larger than in controls. **(B)** Maximal projection of spread spheroids labelled for F-actin with Phalloidin, shown as FIRE LUT. (B') Profiles obtained from xz and yz orthogonal projections. Top panels show the two profiles of the spheroid, bottom panel an enlarged view. The middle diagram schematizes the characteristic morphology of the three conditions. The red dashed line indicates the emerging dome. **(C)** Quantification. The area increase (C') was not significantly different. The ratio between the visible dome and the total area (C') was strongly decreased in EpCAM KD and increased in Trop2 KD. 30-33 spheroids from 4 experiments. Refer to S1 Data. One-way non-parametric ANOVA (Kruskal-Wallis Test) followed by Dunn post-hoc test. **(D)** EpCAM and Trop2 immunofluorescence of wild type MDA-MD-453 cells densely seeded on collagen gel. Slices of the ventral, medial and dorsal planes are shown, with the outlines of one cell indicated by a dotted line. (D') Profile obtained from orthogonal slices, maximum projection of 5 slices. Arrow: ventral interface; filled arrowhead: lateral surface; concave arrowhead: dorsal side. **(E,E')** Dorsal/ventral ratio of EpCAM and Trop2 intensities shows that EpCAM is enriched dorsally and Trop2 ventrally. Quantification of 33 cells from 3 experiments. Dots: Averages of individual experiments. E' shows the pair of ratios for each cell. Red line indicates the single cell where the ratios were inverted. Refer to S1 Data. Statistical analysis using Student's t-test. Scale bars: A,B, 50µm; D, 5µm.

Discussion

We uncovered in this study an unexpectedly subtle regulatory system that has a major impact on adhesive and migratory properties. EpCAM and Trop2 are very closely related proteins with almost identical properties, and we validated here that when expressed in the same cells, they both acted as negative regulators of myosin activity, working toward the same goal of moderating global cell contractility, as seen through quantification of cortical pMLC and firmly demonstrated by our TFM data. Nevertheless, depleting one or the other yielded to diametrically opposed phenotypes, indicating that these quasi twin molecules function as a mechanostat in tissue morphogenesis. While we have discovered and characterized in detail this surprising phenomenon in MCF7 cells, we also found confirming evidence in two other breast cancer cell lines, which suggests that this is a general property of this pair of molecules.

The most striking phenotype resulting from changing EpCAM or Trop2 levels is an opposite effect on spreading, consistently observed for single cells, groups and spheroids, and in the three cell lines. This effect is clearly linking EpCAM and Trop2 to a role in modulating substrate wetting [39,41], thus in acting on the balance of cortical tensions [40]. We should clarify at this point that, while actin polymerization-based protrusive activity can also participate to cell spreading and is certainly an essential component for cell migration, we see this aspect as being at most peripherally associated with the EpCAM and Trop2-dependent phenotypes. In MCF7 cells, dynamic protrusions were observed in all situations and any degree of cell spreading, from flat EpCAM KD cells to round Trop2 KD cells. Furthermore, it would be hard to reconcile with the supracellular effect on spreading of whole spheroids. As for HCC1500 cells, most did not even form lamellipodia on collagen gel, and EpCAM depletion induced spreading of the cell "body", generally in the absence of detectable "protrusions", as evident from the z profiles. Another striking feature observed in our EpCAM and Trop2 KD experiments was the impact on cell-cell adhesion and tissue cohesion, which appeared to follow the same trend in the three different cell lines. As introduced in Box 1, cell adhesion is also a phenomenon of cell wetting, here cells maximizing their common interface. These observations amply support the view that cortical actomyosin contractility is the major target of EpCAM and Trop2 as far as cell behavior is concerned.

At first glance, the increased spreading and cohesion of EpCAM depleted MCF7 cells may seem at odds with the proadhesive role of EpCAM observed in low vertebrate embryos and human intestinal cells [10,12,13,27–29]. We had predicted that the consequences on cell behaviour shall be context-dependent [12], contractility being on one side antagonistic to adhesion [40], on the other side essential to stabilize and reinforce adhesion [59], a duality that considerably broadens the possible phenotypes (Box 1). However, the opposite EpCAM and Trop2 phenotypes in breast cancer cells came as a surprise. We propose that we are here dealing with two levels of regulation.

The first level concerns that capacity of adhesive structures to cope with increased cortical tension: In the case of fish and Xenopus and human intestinal cells, cell-cell contacts were unable to resist to the burst in cortical tension caused by EpCAM depletion, which led to loss of tissue integrity. In breast cancer cells, however, the higher tension experienced upon depletion of either EpCAM, Trop2, or even both, appeared to be at least partially compensated by cadherin recruitment, a sign of adhesion reinforcement. This reaction was particularly spectacular in the case of EpCAM-depleted MCF7 spheroids, which manage the feat of strongly expanding, maintaining high tissue cohesion while allowing extensive amount of intratissue cell movements (intercalation) required for their spreading. Whether these different responses depend on the absolute levels of tension exerted on adhesive structures or on intrinsic cell-type dependent responses remains to be explored.

The second level concerns the unexpected opposite phenotypes observed in these human cell lines expressing both EpCAM and Trop2. By accurately dissecting this system at the tissue and single cell level, we can propose a model that solves at least part of this riddle. We could relate the single cell and spheroid spreading and adhesive phenotypes to differences in the balance between tension at the various interfaces, and we propose that partial differential distribution of EpCAM, which has a slight preference for the free cell edge, and Trop2, more enriched at contact interfaces, may be sufficient to explain their antagonistic roles. Modelling the actual

Figure 13

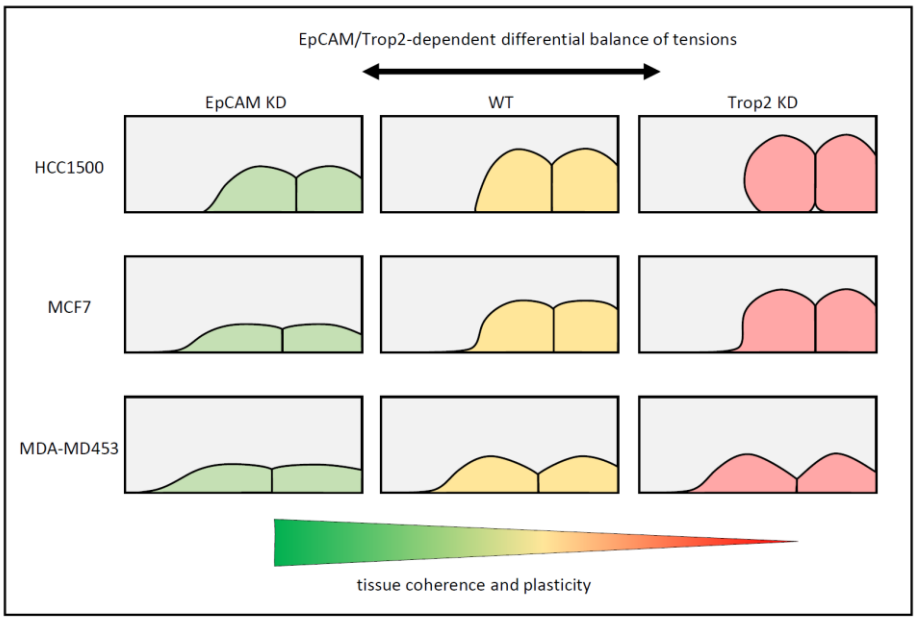

Figure 13. Similarities in EpCAM and Trop2 KD phenotypes in the three breast cancer cell lines tested in this study. HCC1500, MCF7 and MDA-MD-453 are all luminal breast cancer cell lines that share in common the ability to form E-cadherin cell-cell contacts, but differ in their ability to spread on a collagen matrix ("wetting"). Cell-cell adhesion, thus tissue cohesion, appears to dominate over matrix adhesion for HCC1500, while for MDA-MD-453 the balance is tilted the other way. MCF7 represent an intermediate case. In all three cell lines, EpCAM KD tends to stimulate both spreading on the matrix AND cell-cell adhesion/tissue cohesion (flatter angles at contact vertices), while Trop2 KD tends on the contrary to increase tension at both types of interfaces.

tensions measured for wild type and depleted cells confirmed that relatively small variations in the balance of cellular tensions could indeed have a large effect on the final behavioral output. Simple considerations on the relative impact of the three tensions γ_m, γ_c and γ_x provides an explanatory logic for most phenotypes observed in this study, both for single cells and spheroids: In the simple case of isolated cells, a large portion of their surface exposed to the medium, the rest being in contact with the matrix. Their behaviour is then controlled by γ_m and γ_x. In a cell mass, however, a large fraction of the cells is buried in the core, fully surrounded by other cells, thus γ_c dominates. Only those cells exposed to the surface are under the influence of the γ_c/γ_m balance. Cells at the base of the spheroid are subjected to γ_c and γ_x, and those at the edge of the spreading spheroid to all three tensions. This is sufficient to explain why the core of the wild type spheroids remains compact, while cells at the edge can bulge out and even detach, driven by their ability to migrate on the matrix. It also explains for instance the differences in the effect of EpCAM KD for single cells and spheroids: For the former, high spreading and increased cortical tension favoured formation of radially oriented protrusions pulling symmetrically in all directions, which led to their immobilization. In spheroids, the same EpCAM-depleted cells could actively spread collectively. Here, cells exposed at the margin of the aggregate will undergo an inevitable symmetry breaking, which is sufficient to explain directional migration [60].

Comparison of the other cell lines offered a preliminary glance at the spectrum of behaviours that can be achieved by the combined activity of the two partly redundant and partly antagonistic regulators (Fig 13). It shows different flavours of EpCAM and Trop2 LOF phenotypes, which appear directly related to the basal properties of each cell type. We propose that EpCAM and Trop2 modulate cell behaviour without necessarily overturning the intrinsic cell characteristics. HCC1500 cells, for instance, spread very poorly on collagen, and while they do spread slightly better upon EpCAM KD, they are definitely not transformed into a mesenchymal-type cell. Conversely, in the case of the much less coherent MDA-MD-453 cells, EpCAM KD or Trop2 KD influence spheroid compaction, but do not significantly affect their fast expansion. EpCAM and Trop2 LOF phenotypes were most spectacular in MCF7 cells, presumably because these cells are in a regime which is close

to a turning point, where moderate changes in tension can significantly tilt single cell as well as collective behaviour.

While we find quite enticing that such spectacular phenotypes may be explained by slight differences in the local balance of cortical contractility, we should not exclude other alternate or complementary possibilities, including differences in biochemical activities of the two proteins. At the moment, however, myosin downregulation is the only firmly validated property related to morphogenetic properties, but future studies may provide additional mechanisms.

Another important question that should be investigated is the molecular basis of the differential activity of EpCAM and Trop2. We have determined here differences in their localization, consistent with stronger impact on specific interfaces. However, this description is certainly incomplete, and we suspect the existence of deeper differences behind these subtle enrichments. Clear hints include the strong sensitivity of Trop2 IF signal to detergents, and the related discrepancy between the apparent equal distribution of EpCAM and Trop2 at outer cell-cell contacts in non-permeabilized cells, contrasting with the relative depletion of Trop2 in permeabilized samples. We postulate the existence of distinct pools within the plasma membrane, displaying either different activities, or perhaps simply different levels of activity. One lead is the known capacity of EpCAM to assemble into oligomers [61]. Additional avenues include association with tetraspanin-based domains (TEM), as well as with members of the claudin family, which are well documented for EpCAM [62,63]. While Trop2 appears to have similar associations [33,64], one could easily imagine some degree of specificity at this level. Various other interactions have been proposed, including with the actin cytoskeleton [6,64,65], although they are in need of further validation. A related puzzling issue raised by our result is the unilateral dependency of Trop2 for EpCAM, both in terms of level and subcellular localization. While EpCAM and Trop2 both form homodimers, structural considerations indicate incompatibility for heterodimers [66]. Nevertheless, Trop2 could be recruited and stabilized in other ways, e.g. to EpCAM larger oligomers or TEMs [6,11,61–63]. Alternatively, Trop2 could be "protected" by EpCAM competing for targeting and/or degradative routes mechanisms.

One should also note that the LOFs of EpCAM or Trop2 achieved in this study were acute (over a couple of days), and it could be conceivable that, on the longer term, cells adapt to this loss by rerouting the remaining partner. This would explain the apparent redundancy observed for embryonic development of single knock-out mice [67–69]. A recent study supports this notion, as it shows that loss of one Trop2 allele (+/- heterozygotes) was sufficient to aggravate EpCAM -/- KO, leading to high embryonic lethality [33]. The same study further highlighted partial compensation between EpCAM and Trop2 in tissues where both are expressed [33]. Note that in the case of human CTE, tuft formation in the small intestine caused by mutations in EpCAM was only partially rescued by Trop2 expression [34]. Based on the results of the present study, it is plausible that Trop2 may only be able to rescue the shared global action on contractility, but EpCAM may be specifically required to insure the correct structure and homeostasis of the intestinal epithelium. We consider that the depletion/overexpression approach used in this study, although obviously prone to the caveats inherent to any LOF/GOF experiments, had here a clear physiological relevance, since the magnitude of the changes in EpCAM and Trop2 levels was compatible with what happens during cancer development. MCF7 cells represent in this regard a good model, based on the elevated expression levels compared to normal epithelia as well as on the abrupt drop in EpCAM expression observed after EMT [15]. While this study has only addressed the function of EpCAM and Trop2 in three cell lines in an *in vitro* context, we hypothesize that co-expression of EpCAM and Trop2 may act as a general mechanostat contributing in setting the adhesive and migratory properties, which may be broadly relevant in the context of the biology of carcinoma. Indeed, significant levels of both EpCAM and Trop2 are found in a large number of cancer cell lines and multiple types of human cancers (Expression Atlas, https://www.ebi.ac.uk/gxa/ and Protein Atlas https://www.proteinatlas.org/). Our data highlight the capacity of EpCAM and Trop2 to elicit distinct behaviours under different situations, explaining why one cannot assign a general unambiguous pro- or anti-invasive activity to these molecules. Rather, our results provide a framework for more refined analyses and interpretations of their contextual role in normal tissues and in cancer. For instance, changes in their expression is predicted to differentially affect cells located within a tumour and cells positioned at its edge. In the latter

case, the presence of EpCAM and/or Trop2 may well be pivotal for the fate of those cells that, in response to other parameters, may be already on the verge of escaping. Similarly, for cells that have already undergone invasion, the impact of EpCAM and Trop2 expression will differ for single cells versus groups of cells undergoing collective migration. In this context, we find it particularly intriguing that EpCAM expression promotes cell escape from a compact tissue, and that Trop2 depletion in an EpCAM-positive tissue favours detachment of cell groups. While such events were only observed at low frequency in the non-invasive MCF7 cell line, regulation of EpCAM levels could play a more prominent role under conditions corresponding to the early stage of transition to metastasis. Finally, the EpCAM/Trop2 pair must be viewed as part of a much larger system of multiple mechanisms, all contributing to set tensile forces, adhesion and motility. How their morphogenetic potentials identified in the present study are integrated within this complex network is an exciting topic for future studies.

Material and methods

Cell culture. MCF-7, HCC1500 and MDA-MD-453 cells, originally acquired from ATCC, were provided by the SIRIC Montpellier center, courtesy of Dr. Marion Lapierre. They were grown in complete culture medium, i.e. Dulbecco's modified Eagle's medium (DMEM) with 4.5 g/l glucose, supplemented with 10% fetal bovine serum (FBS), 1% antibiotic-antimycotic and 1% non-essential amino acids (all Gibco/Thermo Fischer Scientific), at 37°C and 5% CO_2, for a maximum of 10 passages. 0.05% Trypsin-EDTA (Gibco/Thermo Fischer Scientific) was used for dissociation and passage.

Antibodies, reagents, and solutions. The list of antibodies and dilutions used for IF are presented in Table 1. Secondary antibodies and phalloidin conjugated to Alexa fluorophores were from Molecular Probes/Thermo Fischer Scientific. EpCAM (sc-43032), Trop2 (sc-72392) and control non-targeting (sc-37007) siRNA were from Santa Cruz Biotechnology. A second Trop2 siRNA (H502-0033) was obtained from Sigma/Merck. Mitomycin C was from Sigma/Merck (M4287). Calphostin and Blebbistatin from EMD/Millipore. The EdU click reaction kit with Alexa Fluor 488 dye was from Invitrogen/Thermo Fisher Scientific (C10337). Phosphate Buffer Saline (PBS) without calcium and magnesium was from EuroBio (CS1PBS01-01). Tris Buffer Saline (TBS) was 100mM Tris-HCl pH 7.2, 150mM NaCl. Dissociation buffer was 88mM NaCl, 1mM KCl and 10mM NaHCO3, pH = 9.5 [50].

Table 1. List of antibodies

Antigen	Antibody name	Species	Supplier and cat #	Dilution
EpCAM	323/A3	Mouse	Sant Cruz Biotechnology	1:1000
Trop2	MA5	Rabbit	MA5-29593, Invitrogen/Thermofisher	1:1000
pMLC	(Ser19) pMLC	Mouse	3675, Cell Signaling	1:200
pMLC	(Ser19) pMLC	Rabbit	AB3381, Millipore	1:1000
E-cadherin	24E10	Mouse	3195, Cell Signaling	1:400
vinculin	MA1103	Mouse	Boster Bio	1:100
GFP	GFP-1020	Chicken	Aves Labs	1:1000

siRNA transfection. Cells were seeded in 24-well plates at 0.2×10^6 density one day before siRNA transfection, and 1.6ml fresh medium was added just before transfection. 40 picomoles siRNA (2x 40 picomoles for dKD) and of 4µl Lipofectamine RNAiMAX (8µl for kD) (Invitrogen/Thermo Fischer Scientific) were added to each well. Efficient KD was obtained after 48 to 72 hours.

Fibrillar collagen gels. Glass bottom dishes (Cellvis, D35-20-1.5-N) or 12mm round coverslips were plasma cleaned to create a hydrophilic surface, then coated at 4°C with a thin layer of a 2mg/ml solution of collagen I (from a ~3mg/ml stock solution in 0.02N acetic acid) in PBS, titrated to alkalinity by addition of NaOH, and incubated at 37 °C for 30 min for gelling.

Spheroid formation. The siRNA transfected cells were dissociated by trypsin and counted using trypan-blue solution and an automated cell counter (Invitrogen, Countess). For each spheroid, 400 cells were suspended in 200 µl complete culture medium containing 20% methylcellulose (Sigma, M0262-100G) and incubated in single wells of round-bottom 96-well plates (Greiner Bio-One Cellstar, 650185) for 48hrs.

Spheroid migration assay. The formed spheroids were transferred to glass-bottom dishes coated with collagen gel. Adherence to the gel was observed within 30 min. Spheroids were imaged with an Olympus IX83 inverted widefield video-microscope controlled by Metamorph software using a 10x (0.3NA) or 20x (0.45NA) objective. Time lapse images were acquired every 30 min for 24hrs.

Single cell migration assay. Cells were dissociated in dissociation buffer and counted as above, 0.5×10^5 cells were plated on top of collage gel and left to adhere for about 3 hours before acquisition of time lapses. Imaging conditions were as for spheroids, with a 20x (0.45NA) objective, every 5 to 7 min for 15 hours. Migration was measured using the MetaMorph software tracking tool.

Immunostaining. Spheroids (in glass-bottom dishes) were fixed for 30 min in 3.7% paraformaldehyde (PFA, #15714, Electron Microscopy Sciences) in PHEM buffer (60mM PIPES, 25mM HEPES, 10mM EGTA, and 4mM MgSO4, pH 7.2), followed by 30 min permeabilization in 1% Triton X100 in PBS. Fixed samples were washed twice with TBS, incubated for 45 min at RT in blocking buffer (20% sheep serum (S2350-100, Biowest) in PBS, followed by overnight at 4°C with primary antibodies and fluorescent phalloidin diluted in PBS with 10% sheep serum, then another overnight with secondary antibodies and Hoechst 33342 (H3570, Invitrogen/Thermo Fischer Scientific, 1:2000), rinsed and kept in PBS. Fixation and immunostaining of cells and groups of cells (on coverslips) were similarly, but with shorter times (10 min fixation, 10 min permeabilization, 1-2 hrs incubation with antibodies, all at RT), and coverslips were mounted using antifade mounting media (Slowfade, S36972, Molecular Probes/Thermo Fischer Scientific). For cell-surface labelling, Triton X100 permeabilization after fixation was skipped, but samples were post-fixed after primary antibody incubation, and permeabilized before incubation with the secondary antibodies.

Confocal microscopy. z-stacks (0.2 to 0.4µm distance between planes) of immunolabelled cells and groups of cells were acquired using an inverted scanning confocal microscope (Leica SP5-SMD), 63x oil objective (1.4NA). Spheroids were imaged using a Nikon inverted microscope coupled to the Andor Dragonfly spinning disk, 40X water objective (1.15NA) as z-stacks of 4 by 4 tile-scans (1µm distance between planes), which where stitched to generate full images of whole spheroids.

Image quantification

All quantifications were performed using ImageJ. In all cases, cytoplasmic signal was taken as background, and subtracted from the corresponding intensity values. For measurement of relative E-Cadherin and pMLC signal intensities of whole-mount labelled spheroids, the membrane signal was obtained from horizontal confocal slices through thresholding after background subtraction. Values were normalized for each experiment to the average signal in control spheroids. For small groups of cells, peak intensities for pMLC and E-cadherin were measured by drawing a line across two adjacent cells, perpendicular to the cell edges, and running the corresponding plot profile function throughout the z stack to select the planes with respectively highest E-cadherin and pMLC peaks at cell-cell contact, and highest pMLC peaks at each free edge. These measurements were repeated for each cell pair of a group. Relative intensities were calculated from the areas of these peaks after background subtraction. Vinculin FA quantification was based on thresholding and measurement of average intensity and FA total surface per cell (or cell group). Integrated intensity was calculated as vinculin average intensity x surface. Normalization to cell size was obtained by dividing by the maximal horizontal cell area. EpCAM and Trop2 relative signals in cell groups were measured as average intensity on line scans drawn along the plasma membrane at defined locations, either on horizontal sections or on z projections produced using the "reslice" function. The detailed locations in MCF7 cells are detailed in S9 Fig. The same quantification based on manual drawing of lines along cell interfaces was also used for all the data on HCC1500 et MDA-MD-453 cells.

Quantification of cell morphology.

MCF7 single cells. Dissociated cells laid on collagen gel were stained with phalloidin and Hoechst and imaged by confocal microscopy. Quantification of cell area was made on maximal horizontal projection, cell height on maximal orthogonal projection after stack reslicing, using ImageJ software.

HCC1550 single cells and groups. Z confocal stacks were resliced, and maximal projections from four orientations were used to evaluate angles made between the edge and the ventral interface (acute, roughly right or weakly acute, obtuse). Multiple combinations were compiled into four categories listed in S11B Fig.

Traction force microscopy. Stock solution for soft polyacrylamide substrates of 5 kPa rigidity containing far-red fluorescent nanobeads (Bangs laboratory, FC02F, 0.19 µm) were prepared by mixing acrylamide 40% (A4058, Sigma) and bis-acrylamide 2% (M1533, Sigma) in DPBS 1X (PBS without Ca & Mg, CS1PBS01-01, Eurobio Scientific) according to documented relative concentrations [70,71]. The thin polyacrylamide-based substrate was polymerized between two different glass coverslips (#631-0162, diameter 32 millimeters, thickness No. 1, VWR) prepared as follows. The first coverslip served as base for the gel. It was cleaned using a plasma cleaner machine, then coated with bind-silane (#GE17-1330-01, Sigma) for 3 to 5 min at RT to ensure the attachment of the gel to the coverslip. The second coverslip served to

transfer the patterned extracellular matrix. It was also first plasma cleaned, then coated with 0.1 mg/ml PLL-PEG (PLL20K-G35-PEG2K, JenKem Technology) solution for 30 min at RT to obtain a passivated surface. It was then washed with distilled water, dried, then burned for 5 min with UV light through a micropatterning chrome photomask (45 by 45 μm custom-designed H shapes, micropatterned onto chrome photomask by Toppan). This allowed adsorption of the collagen coating at the burned sites resulting in a micropatterned coated coverslip. Collagen type-I was added at 0.5mg/ml in 0.02 N acetic acid and left for 45 min at RT. For gel polymerization, 1 μl of 10% ammonium persulfate (A3678, Sigma), 1 μl of TEMED (T9281, Sigma) and 0.35 μl of the above-mentioned nanobeads were added to 165 μl of the acrylamide-bisacrylamide stock solution. 47 μl of this solution were used to put between the two coverslips for polymerization (30 min, RT). Once polymerized, the collagen-coated top coverslip was gently removed, exposing the collagen H micropatterned gel. Cells were plated on this substrate at a density of 0.5×10^5 per coverslip in a culture dish. The medium of each dish was replaced with fresh medium to wash out cells that didn't adhere to the substrate (this step avoided ending up with cells that were not on the patterns). The dishes were then kept in the incubator overnight to allow cell division to obtain cell doublets on each H micropattern. Cells and the underneath nanobeads were imaged using an epifluorescence inverted microscope (Nikon Ti2-E2) with 40x air objective (1.15NA) and an Orca Flash 4.0 sCMOS camera (Hamamatsu), with temperature set at 37°C. This first image served as stressed (pulled) state of the beads. Then the cells were removed from the patterns using trypsin and another image of the same position was taken serving as unstressed state of the beads. The displacement field analysis was done using a custom-made algorithm based on the combination of particle image velocimetry and single-particle tracking. Traction forces were calculated using Fourier transform traction cytometry with zero-order regularization [72,73]. All calculations and image processing were performed using MATLAB software.

Production and analysis of free-floating cell doublets. siRNA transfected cells were dissociated by a 10 min incubation at RT with dissociation buffer. The buffer was then removed, 1 ml of complete culture medium was added to the cells, and single dissociated cells were obtained by pipetting. Dissociated cells of two different conditions (with control cells labelled with Hoechst 33342) were gently mixed, transferred to agarose-coated plastic dishes (2% agarose in PBS) in complete culture medium and put in the incubator for 10 to 15 min to allow partial reassociation. This time was empirically determined as sufficient to reach close to maximal cell-cell contact expansion while minimizing formation of larger groups of cells. Reassociated cells were then gently transferred to a glass-bottom dish coated with a thin layer of 2% agarose, in complete culture medium containing a 1:10000 dilution of the membrane dye CellMask deep red (C1004, Molecular Probes/Thermo Fischer Scientific). Cell doublets were imaged by live confocal microscopy using a Dragonfly spinning disk (Andor) mounted on a Nikon inverted microscope with a 20x (0.75 NA/oil) objective, at 37°C and 5% CO_2. Hoechst and CellMask images were obtained simultaneously using two CCD cameras (EMCCD iXon888 Life Andor). Quantifications of the relative cortical tensions and adhesiveness were done based geometry of cell membranes at the vertices, as previously described [53]. Homo- and heterotypic doublets were identified based on the presence of Hoechst-positive nuclei.

Statistical analysis. All statistical analyses were performed using the Excel real statistics add-in. Unless otherwise stated, experiments were replicated at least three times and comparisons between conditions were done using either one-way ANOVA followed by Tukey-HSD post hoc test, or the non-parametric Kruskal-Wallis Test, followed by Dunn post-hoc test. p values met the following criteria $*p < 0.05$, $**p < 0.01$, and $***p < 0.001$ and NS, not significant.

Acknowledgements

We acknowledge the help of the MRI imaging platform. We thank Marion Lapierre (IRCM Montpellier) for advice and for providing cell lines. This study was supported by ANR grant ANR-14-ACHN-0004–ICM, ANR-21-CE13-0042-01, and a Labex EpiGenMed Chair of excellence ANR grant to F.F., and CIHR grant 130350 to F.F. and P.L.

References

1. Went PT, Lugli A, Meier S, Bundi M, Mirlacher M, Sauter G, et al. Frequent EpCam protein expression in human carcinomas. 2004. Hum Pathol. 2004;35: 122–128.

2. Rao CG, Chianese D, Doyle GV, Miller MC, Russell T, Sanders RA, et al. Expression of epithelial cell adhesion molecule in carcinoma cells present in blood and primary and metastatic tumors. Int J Oncol. 2005;27: 49–57.

3. Gires O, Bauerle PA. EpCAM as a target in cancer therapy. Journal of clinical oncology : official journal of the American Society of Clinical Oncology. 2010;28: e239-40; author reply e241-2. doi:10.1200/JCO.2009.26.8540

4. Litvinov SV, Bakker HA, Gourevitch MM, Velders MP, Warnaar SO. Evidence for a role of the epithelial glycoprotein 40 (Ep-CAM) in epithelial cell-cell adhesion. Cell Adhes Commun. 1994;2: 417–28. doi:10.3109/15419069409004452

5. Balzar M, Prins FA, Bakker HA, Fleuren GJ, Warnaar SO, Litvinov SV. The structural analysis of adhesions mediated by Ep-CAM. Exp Cell Res. 1999;246: 108–21.

6. Fagotto F, Aslemarz A. EpCAM cellular functions in adhesion and migration, and potential impact on invasion: A critical review. Biochimica et Biophysica Acta (BBA)-Reviews on Cancer. 2020;1874: 188436.

7. Gaber A, Lenarcic B, Pavsic M. Current View on EpCAM Structural Biology. Cells. 2020;9. doi:10.3390/cells9061361

8. Maetzel D, Denzel S, Mack B, Canis M, Went P, Benk M, et al. Nuclear signalling by tumour-associated antigen EpCAM. Nat Cell Biol. 2009;11: 162–171.

9. Chaves-Perez A, Mack B, Maetzel D, Kremling H, Eggert C, Harreus U, et al. EpCAM regulates cell cycle progression via control of cyclin D1 expression. Oncogene. 2013;32: 641–50. doi:10.1038/onc.2012.75

10. Barth AIM, Kim H, Riedel-Kruse IH. Regulation of epithelial migration by epithelial cell adhesion molecule requires its Claudin-7 interaction domain. PLoS ONE. 2018;13: e0204957. doi:10.1371/journal.pone.0204957

11. Gaston C, De Beco S, Doss B, Pan M, Gauquelin E, D'Alessandro J, et al. EpCAM promotes endosomal modulation of the cortical RhoA zone for epithelial organization. Nature communications. 2021;12: 2226. doi:10.1038/s41467-021-22482-9

12. Maghzal N, Kayali HA, Rohani N, Kajava AV, Fagotto F. EpCAM Controls Actomyosin Contractility and Cell Adhesion by Direct Inhibition of PKC. Developmental Cell. 2013;27: 263–77. doi:10.1016/j.devcel.2013.10.003

13. Salomon J, Gaston C, Magescas J, Duvauchelle B, Canioni D, Sengmanivong L, et al. Contractile forces at tricellular contacts modulate epithelial organization and monolayer integrity. Nature communications. 2017;8: 13998. doi:10.1038/ncomms13998

14. Fagotto F. EpCAM as Modulator of Tissue Plasticity. Cells. 2020;9: 2128. doi:10.3390/cells9092128

15. Sankpal NV, Fleming TP, Sharma PK, Wiedner HJ, Gillanders WE. A double-negative feedback loop between EpCAM and ERK contributes to the regulation of epithelial-mesenchymal transition in cancer. Oncogene. 2017;36: 3706–3717. doi:10.1038/onc.2016.504

16. Vannier C, Mock K, Brabletz T, Driever W. Zeb1 Regulates E-cadherin and Epcam (Epithelial Cell Adhesion Molecule) Expression to Control Cell Behavior in Early Zebrafish Development. Journal of Biological Chemistry. 2013;288: 18643–18659. doi:10.1074/jbc.M113.467787

17. Pan M, Schinke H, Luxenburger E, Kranz G, Shakhtour J, Libl D, et al. EpCAM ectodomain EpEX is a ligand of EGFR that counteracts EGF-mediated epithelial-mesenchymal transition through modulation of phospho-ERK1/2 in head and neck cancers. PLoS Biol. 2018;16: e2006624. doi:10.1371/journal.pbio.2006624

18. Gao J, Yan Q, Wang J, Liu S, Yang X. Epithelial-to-Mesenchymal Transition Induced by TGF-β1 Is Mediated by AP1-Dependent EpCAM Expression in MCF-7 Cells. Journal of Cellular Physiology. 2015;230: 775–782. doi:10.1002/jcp.24802

19. Wang M-H, Sun R, Zhou X-M, Zhang M-Y, Lu J-B, Yang Y, et al. Epithelial cell adhesion molecule overexpression regulates epithelial-mesenchymal transition, stemness and metastasis of nasopharyngeal carcinoma cells via the PTEN/AKT/mTOR pathway. Cell Death Dis. 2018;9: 1–16. doi:10.1038/s41419-017-0013-8

20. Campbell K, Casanova J. A common framework for EMT and collective cell migration. Development. 2016;143: 4291–4300. doi:10.1242/dev.139071

21. Friedl P, Locker J, Sahai E, Segall JE. Classifying collective cancer cell invasion. Nat Cell Biol. 2012;14: 777–83. doi:10.1038/ncb2548

22. Jolly MK, Mani SA, Levine H. Hybrid epithelial/mesenchymal phenotype(s): The "fittest" for metastasis? Biochim Biophys Acta Rev Cancer. 2018;1870: 151–157. doi:10.1016/j.bbcan.2018.07.001

23. Balcik-Ercin P, Cayrefourcq L, Soundararajan R, Mani SA, Alix-Panabières C. Epithelial-to-Mesenchymal Plasticity in Circulating Tumor Cell Lines Sequentially Derived from a Patient with Colorectal Cancer. Cancers (Basel). 2021;13: 5408. doi:10.3390/cancers13215408

24. Koch C, Kuske A, Joosse SA, Yigit G, Sflomos G, Thaler S, et al. Characterization of circulating breast cancer cells with tumorigenic and metastatic capacity. EMBO Molecular Medicine. 2020;12: e11908. doi:10.15252/emmm.201911908

25. Lenárt S, Lenárt P, Šmarda J, Remšík J, Souček K, Beneš P. Trop2: Jack of All Trades, Master of None. Cancers (Basel). 2020;12: E3328. doi:10.3390/cancers12113328

26. Švec J, Šťastná M, Janečková L, Hrčkulák D, Vojtěchová M, Onhajzer J, et al. TROP2 Represents a Negative Prognostic Factor in Colorectal Adenocarcinoma and Its Expression Is Associated with Features of Epithelial-Mesenchymal Transition and Invasiveness. Cancers (Basel). 2022;14: 4137. doi:10.3390/cancers14174137

27. Slanchev K, Carney TJ, Stemmler MP, Koschorz B, Amsterdam A, Schwarz H, et al. The Epithelial Cell Adhesion Molecule EpCAM Is Required for Epithelial Morphogenesis and Integrity during Zebrafish Epiboly and Skin Development. PLoS Genet. 2009;5: e1000563.

28. Maghzal N, Vogt E, Reintsch W, Fraser JS, Fagotto F. The tumor associated EpCAM regulates morphogenetic movements through intracellular signaling. J Cell Biol. 2010;119: 645–659.

29. Sivagnanam M, Mueller JL, Lee H, Chen Z, Nelson SF, Turner D, et al. Identification of EpCAM as the gene for congenital tufting enteropathy. Gastroenterology. 2008;135: 429–37. doi:10.1053/j.gastro.2008.05.036

30. Osta WA, Chen Y, Mikhitarian K, Mitas M, Salem M, Hannun YA, et al. EpCAM Is Overexpressed in Breast Cancer and Is a Potential Target for Breast Cancer Gene Therapy. Cancer Res. 2004;64: 5818–5824. doi:10.1158/0008-5472.can-04-0754

31. Dai X, Cheng H, Bai Z, Li J. Breast cancer cell line classification and its relevance with breast tumor subtyping. Journal of Cancer. 2017;8: 3131.

32. Wu CJ, Lu M, Feng X, Nakato G, Udey MC. Matriptase Cleaves EpCAM and TROP2 in Keratinocytes, Destabilizing Both Proteins and Associated Claudins. Cells. 2020;9. doi:10.3390/cells9041027

33. Szabo R, Ward JM, Artunc F, Bugge TH. EPCAM and TROP2 share a role in claudin stabilization and development of intestinal and extraintestinal epithelia in mice. Biology Open. 2022;11: bio059403. doi:10.1242/bio.059403

34. Nakato G, Morimura S, Lu M, Feng X, Wu C, Udey MC. Amelioration of Congenital Tufting Enteropathy in EpCAM (TROP1)-Deficient Mice via Heterotopic Expression of TROP2 in Intestinal Epithelial Cells. Cells. 2020;9: 1847. doi:10.3390/cells9081847

35. Kramer N, Walzl A, Unger C, Rosner M, Krupitza G, Hengstschläger M, et al. In vitro cell migration and invasion assays. Mutat Res. 2013;752: 10–24. doi:10.1016/j.mrrev.2012.08.001

36. Insua-Rodríguez J, Oskarsson T. The extracellular matrix in breast cancer. Advanced drug delivery reviews. 2016;97: 41–55.

37. Steinberg MS. Reconstruction of tissues by dissociated cells. Some morphogenetic tissue movements and the sorting out of embryonic cells may have a common explanation. Science. 1963;141: 401–8.

38. Harris AK. Is Cell sorting caused by differences in the work of intercellular adhesion? A critique of the Steinberg hypothesis. J Theor Biol. 1976;61: 267–285.

39. Ryan PL, Foty RA, Kohn J, Steinberg MS. Tissue spreading on implantable substrates is a competitive outcome of cell–cell vs. cell–substratum adhesivity. Proc Natl Acad Sci USA. 2001;98: 4323–4327. doi:10.1073/pnas.071615398

40. Brodland GW. The Differential Interfacial Tension Hypothesis (DITH): a comprehensive theory for the self-rearrangement of embryonic cells and tissues. Journal of biomechanical engineering. 2002;124: 188–97.

41. Douezan S, Guevorkian K, Naouar R, Dufour S, Cuvelier D, Brochard-Wyart F. Spreading dynamics and wetting transition of cellular aggregates. Proc Natl Acad Sci USA. 2011;108: 7315–7320. doi:10.1073/pnas.1018057108

42. Amack JD, Manning ML. Knowing the boundaries: extending the differential adhesion hypothesis in embryonic cell sorting. Science. 2012;338: 212–5. doi:10.1126/science.1223953

43. Winklbauer R. Cell adhesion strength from cortical tension - an integration of concepts. J Cell Sci. 2015;128: 3687–93. doi:10.1242/jcs.174623

44. Engl W, Arasi B, Yap LL, Thiery JP, Viasnoff V. Actin dynamics modulate mechanosensitive immobilization of E-cadherin at adherens junctions. Nat Cell Biol. 2014;16: 584–591. doi:10.1038/ncb2973

45. Gao X, Acharya BR, Engl WCO, De Mets R, Thiery JP, Yap AS, et al. Probing compression versus stretch activated recruitment of cortical actin and apical junction proteins using mechanical stimulations of suspended doublets. APL Bioengineering. 2018;2: 026111. doi:10.1063/1.5025216

46. David R, Luu O, Damm EW, Wen JW, Nagel M, Winklbauer R. Tissue cohesion and the mechanics of cell rearrangement. Development. 2014;141: 3672–82. doi:10.1242/dev.104315

47. Leckband DE, de Rooij J. Cadherin Adhesion and Mechanotransduction. Annu Rev Cell Dev Biol. 2014;30: 291–315. doi:10.1146/annurev-cellbio-100913-013212

48. Tseng Q, Duchemin-Pelletier E, Deshiere A, Balland M, Guillou H, Filhol O, et al. Spatial organization of the extracellular matrix regulates cell-cell junction positioning. Proc Natl Acad Sci U S A. 2012;109: 1506–11. doi:10.1073/pnas.1106377109

49. Ruppel A, Wörthmüller D, Misiak V, Kelkar M, Wang I, Moreau P, et al. Force propagation between epithelial cells depends on active coupling and mechano-structural polarization. Kruse K, Cooper JA, editors. eLife. 2023;12: e83588. doi:10.7554/eLife.83588

50. Canty L, Zarour E, Kashkooli L, Francois P, Fagotto F. Sorting at embryonic boundaries requires high heterotypic interfacial tension. Nature communications. 2017;8: 157. doi:10.1038/s41467-017-00146-x

51. Parent SE, Barua D, Winklbauer R. Mechanics of Fluid-Filled Interstitial Gaps. I. Modeling Gaps in a Compact Tissue. Biophys J. 2017;113: 913–922. doi:10.1016/j.bpj.2017.06.062

52. Fagotto F. Tissue segregation in the early vertebrate embryo. Seminars in cell & developmental biology. 2020;107: 130–146. doi:10.1016/j.semcdb.2020.05.020

53. Kashkooli L, Rozema D, Espejo-Ramirez L, Lasko P, Fagotto F. Ectoderm to mesoderm transition by down-regulation of actomyosin contractility. PLoS Biol. 2021;19: e3001060. doi:10.1371/journal.pbio.3001060

54. Rohani N, Parmeggiani A, Winklbauer R, Fagotto F. Variable combinations of specific ephrin ligand/Eph receptor pairs control embryonic tissue separation. PLoS Biol. 2014;12: e1001955. doi:10.1371/journal.pbio.1001955

55. Graner F, Glazier JA. Simulation of biological cell sorting using a two-dimensional extended Potts model. Physical review letters. 1992;69: 2013–2016.

56. Glazier JA, Graner F. Simulation of the differential adhesion driven rearrangement of biological cells. Phys Rev E Stat Phys Plasmas Fluids Relat Interdiscip Topics. 1993;47: 2128–2154.

57. Izaguirre JA, Chaturvedi R, Huang C, Cickovski T, Coffland J, Thomas G, et al. COMPUCELL, a multi-model framework for simulation of morphogenesis. Bioinformatics. 2004;20: 1129–1137. doi:10.1093/bioinformatics/bth050

58. Cickovski TM, Huang C, Chaturvedi R, Glimm T, Hentschel HGE, Alber MS, et al. A framework for three-dimensional simulation of morphogenesis. IEEE/ACM Trans Comput Biol Bioinform. 2005;2: 273–288. doi:10.1109/TCBB.2005.46

59. Charras G, Yap AS. Tensile Forces and Mechanotransduction at Cell-Cell Junctions. Curr Biol. 2018;28: R445–R457. doi:10.1016/j.cub.2018.02.003

60. Mayor R, Etienne-Manneville S. The front and rear of collective cell migration. Nat Rev Mol Cell Biol. 2016;17: 97–109. doi:10.1038/nrm.2015.14

61. Balzar M, Briaire-de Bruijn IH, Rees-Bakker HAM, Prins FA, Helfrich W, de Leij L, et al. Epidermal Growth Factor-Like Repeats Mediate Lateral and Reciprocal Interactions of Ep-CAM Molecules in Homophilic Adhesions. Mol Cell Biol. 2001;21: 2570–2580. doi:10.1128/mcb.21.7.2570-2580.2001

62. Kuhn S, Koch M, Nubel T, Ladwein M, Antolovic D, Klingbeil P, et al. A complex of EpCAM, claudin-7, CD44 variant isoforms, and tetraspanins promotes colorectal cancer progression. Mol Cancer Res. 2007;5: 553–67. doi:10.1158/1541-7786.MCR-06-0384

63. Nubel T, Preobraschenski J, Tuncay H, Weiss T, Kuhn S, Ladwein M, et al. Claudin-7 regulates EpCAM-mediated functions in tumor progression. Mol Cancer Res. 2009;7: 285–99. doi:10.1158/1541-7786.MCR-08-0200

64. Guerra E, Relli V, Ceci M, Tripaldi R, Simeone P, Aloisi AL, et al. Trop-2, Na+/K+ ATPase, CD9, PKCα, cofilin assemble a membrane signaling super-complex that drives colorectal cancer growth and invasion. Oncogene. 2022;41: 1795–1808. doi:10.1038/s41388-022-02220-1

65. Balzar M, Bakker HA, Briaire-de-Bruijn IH, Fleuren GJ, Warnaar SO, Litvinov SV. Cytoplasmic tail regulates the intercellular adhesion function of the epithelial cell adhesion molecule. Mol Cell Biol. 1998;18: 4833–43.

66. Pavšič M. Trop2 Forms a Stable Dimer with Significant Structural Differences within the Membrane-Distal Region as Compared to EpCAM. IJMS. 2021;22: 10640. doi:10.3390/ijms221910640

67. Lei Z, Maeda T, Tamura A, Nakamura T, Yamazaki Y, Shiratori H, et al. EpCAM contributes to formation of functional tight junction in the intestinal epithelium by recruiting claudin proteins. Dev Biol. 2012;371: 136–45. doi:10.1016/j.ydbio.2012.07.005

68. Guerra E, Lattanzio R, La Sorda R, Dini F, Tiboni GM, Piantelli M, et al. mTrop1/Epcam knockout mice develop congenital tufting enteropathy through dysregulation of intestinal E-cadherin/beta-catenin. PLoS ONE. 2012;7: e49302. doi:10.1371/journal.pone.0049302

69. Wang J, Zhang K, Grabowska D, Li A, Dong Y, Day R, et al. Loss of Trop2 promotes carcinogenesis and features of epithelial to mesenchymal transition in squamous cell carcinoma. Mol Cancer Res. 2011;9: 1686–95. doi:10.1158/1541-7786.MCR-11-0241

70. Tse JR, Engler AJ. Preparation of hydrogel substrates with tunable mechanical properties. Curr Protoc Cell Biol. 2010;Chapter 10: Unit 10.16. doi:10.1002/0471143030.cb1016s47

71. Vignaud T, Ennomani H, Thery M. Polyacrylamide hydrogel micropatterning. Methods in cell biology. Elsevier; 2014. pp. 93–116.

72. Sabass B, Gardel ML, Waterman CM, Schwarz US. High Resolution Traction Force Microscopy Based on Experimental and Computational Advances. Biophysical Journal. 2008;94: 207–220. doi:10.1529/biophysj.107.113670

73. Milloud R, Destaing O, de Mets R, Bourrin-Reynard I, Oddou C, Delon A, et al. αvβ3 integrins negatively regulate cellular forces by phosphorylation of its distal NPXY site. Biol Cell. 2017;109: 127–137. doi:10.1111/boc.201600041

Supplemental material

Annex. Description of simulation (cellular Potts model).
Figure S1. Related to Fig 1.
Figure S2. Related to Fig 1.
Figure S3. Related to Fig 1.
Figure S4. Related to Fig 3.
Figure S5. Related to Fig 3.
Figure S6. Related to Fig 5.
Figure S7. Related to Fig 6 and Fig 9.
Figure S8. Related to Fig 7.
Figure S9. Related to Fig 8.
Figure S10. Related to Fig 8.
Figure S11. Related to Fig 9.
Figure S12. Related to Fig 10.
Figure S13. Related to Fig 12.
Movie 1. Related to Figure 1A.
Time lapse of spreading of siCtrl spheroid on fibrillar collagen.
Movie 2. Related to Figure 1A.
Time lapse of spreading of siEpCAM spheroid on fibrillar collagen.
Movie 3. Related to Figure 1A.
Time lapse of spreading of siTrop2 spheroid on fibrillar collagen.
Movie 4. Related to Figure 1A.
Time lapse of spreading of dKD spheroid on fibrillar collagen.
Movie 5. Related to supplemental Figure 2A.
Time lapse of migration of single siCtrl cell on fibrillar collagen.
Movie 6. Related to Figure 2A.
Time lapse of migration of single siEpCAM cell on fibrillar collagen.
Movie 7. Related to Figure 2A.
Time lapse of migration of single siTrop2 cell on fibrillar collagen.
Movie 8. Related to Figure 2A.
Time lapse of migration of single dKD cell on fibrillar collagen.
Movie 9. Related to Figure 7.
Time lapse of simulation of spheroid spreading on the matrix substrate (blue) using 3D Cellular Potts Model. 3D view.
Movie 10. Related to Figure 7.
Simulation of spheroid spreading on the matrix substrate. Top: xz projection. Bottom: xy projection, plane closest to the substrate.
Movie 11. Related to supplemental Figure 9.
Partial view of control spheroid spreading with detachment of a single cell.
Movie 12. Related to supplemental Figure 9.
Partial view of siEpCAM spheroid spreading, without cell detachment.
Movie 13. Related to supplemental Figure 9.
Partial view of siTrop2 spheroid spreading with detachment of a pair of cells.
Movie 14. Related to supplemental Figure 9.
Partial view of dKD spheroid spreading, without cell detachment.